

Date: September 16, 2017

Gamma-Ray Burst Spectral Correlations: Photospheric and Injection Effects

Felix Ryde

Stockholm Observatory, AlbaNova, SE-106 91 Stockholm, Sweden and Department of Astronomy & Astrophysics, Pennsylvania State University, University Park, PA 16802, USA

Claes-Ingvar Björnsson

Stockholm Observatory, AlbaNova, SE-106 91 Stockholm, Sweden

Yuki Kaneko

Universities Space Research Association, National Space Science and Technology Center, Huntsville, AL, 35805, USA

Peter Mészáros

Department of Astronomy & Astrophysics, Pennsylvania State University, University Park, PA 16802, USA and Department of Physics, Pennsylvania State University, University Park, PA 16802, USA

Robert Preece

Physics Department, University of Alabama in Huntsville, National Space Science and Technology Center, Huntsville, AL 35899, USA

Milan Battelino

Stockholm Observatory, AlbaNova, SE-106 91 Stockholm, Sweden

ABSTRACT

We present a physical framework that can account for most of the observed spectral properties of the prompt gamma-ray burst emission. This includes the variety of spectral shapes, shape evolutions, and spectral correlations between flux and spectral peak, within bursts described by Borgonovo & Ryde, and among

bursts described by Amati/Ghirlanda. In our proposed model the spectral peak is given by the photospheric emission from a relativistic outflow for which the horizon length is much smaller than the radial width. The observed duration of the thermal flash will be given by the radial light-crossing time. This then gives that the typical emission site is at $\sim 10^{11}$ cm from the center, with a Lorentz factor of ~ 300 . This emission is accompanied by non-thermal emission from dissipation locations outside the photosphere. The relative strength of these two components depend on injection effects at the central engine leading to varying relative location of the saturation and photospheric radii. The total emission can then reproduce the observed variety. The spectral correlations are found by assuming that the amount of energy dissipated depends non-linearly on the averaged particle density. Beside the spectral correlations this also gives a description of how the relative strength of the thermal component varies with temperature within a burst.

Subject headings: gamma rays: bursts — gamma rays: observations — radiation mechanisms: nonthermal

1. Introduction

The emission below the spectral peak in gamma-ray bursts (GRBs), which typically lies at around 200 – 300 keV, is indicative of the radiative process in charge of the spectrum formation. In this sense a truly crucial observation is that the power-law slope of the sub-peak emission in a fair fraction of observed, instantaneous spectra are harder than what is expected from optically-thin synchrotron emission (Preece 2000). Indeed, the *Compton Gamma Ray Observatory* BATSE instrument [25–2000 keV] recorded spectra which were as hard as a thermal emission throughout the burst (Ryde 2004) as well as during the initial interval of bursts (Ghirlanda 2003; Ryde 2004; Kaneko 2005; Bošnjak 2005). Furthermore, *Beppo-SAX* [2–700 keV] detected several bursts which exhibited very hard low-energy spectra (see e.g. Frontera et al. (2000)).

Moreover, observations made by *Ginga* [\sim 2–400 keV] (Strohmayer et al. 1998) indicated a substantial number of bursts with breaks below 10 keV, i.e., below the observable range of BATSE. The authors suggested that bursts might have two different spectral breaks, one in the BATSE range and one below this, close to 5 keV. Similar results are reported by *Swift* [0.3–500 keV, with *KONUS*] for GRB050820A (Osborne et al. 2005) whose spectrum indicates that there can be an additional spectral break around 10 keV. These evidence indicate that the high-energy spectra of GRBs are more complicated than that of a single

broken power-law. Similarly, the need for additional high-energy spectral components beyond 1 MeV in several bursts (e.g. Hurley et al. (1994); Atkins et al. (2000); González et al. (2003)) reinforces the same conclusions.

Another crucial point was raised by Ryde (2005) who argued that a strong thermal component could very well be a common feature in the γ -ray spectra of GRBs. Most of the strong, pulsed bursts analyzed could be described by a two-component model consisting of a thermal component, modelled by a Planck function, and a non-thermal component, modelled by a power-law function, the sum of which creates the observed spectral shapes and evolutions. The typical peak in a GRB spectrum is thus argued to be caused by a thermal component. The behaviors of the two separate components on their own are, in general, similar from burst to burst, even though the combined behavior leads to the large variety in spectral evolutions that is observed. The typical behavior of the temperature over a single pulse episode is, with a few exceptions, that it decreases monotonically as a broken power-law in time. The non-thermal emission component, which is parameterized by a power-law photon-index $s \equiv d \log N_E / d \log E$, where N_E is the photon flux, exhibits a typical decrease in s from approximately -1.5 to approximately -2 . Other behaviors do occasionally exist (see Ryde et al. in prep.) These results also hold for bursts which are consistent with optically-thin synchrotron emission, in the sense that spectral fits with a broken power-law function gives a photon-index of the low-energy power-law which is smaller (softer) than $\alpha = -2/3$.

Such thermal–non-thermal hybrid emission is indeed common in astrophysical sources and is a natural consequence of heating of a background plasma and acceleration of particles. This is, for instance, typical for solar flares, accretion disks and cluster of galaxies (see, e.g., Petrosian & Liu 2004). In the case of GRBs, the thermal component is thought to stem from the fireball photosphere while the non-thermal component stems from accelerated electrons beyond the photospheric radius, in the optically-thin region. We will denote this model as the photosphere model since the main feature of it, its energy flux peak, and spectral evolution is given by the thermal component. This certainly emanates from the photosphere, where the optical depth is unity, even though the finally observed emission can be altered due to scattering and diffusion effects.

If we are indeed observing the photospheric, thermal emission, as suggested by the analyses above, it simplifies the physical interpretation since we are detecting the fireball and its evolution directly. This is in contrast to the internal shocks which give us indirect information through the dissipation processes, randomly distributed through out the fireball wind, which by necessity complicates the interpretation. However, the origin of the thermal component and its observed evolution is not obvious. Strong photospheric components were

predicted in the spectra of GRBs, in kinetic models by Mészáros, & Rees (2000); Mészáros et al. (2002); Daigne & Mochkovitch (2002); Ryde (2004), and in Poynting-flux dominated models by e.g. Drenkhahn & Spruit (2002). More recently, discussions on various scenarios and theoretical aspects have been given by, e.g., Rees & Mészáros (2005); Thompson (2005); Pe’er et al. (2005); Thompson, Mészáros, & Rees (2006). In this paper we will assume that the thermal component is predominantly from close to the photosphere and that the evolution we detect is mainly due to change in the property of the photosphere. First, we discuss the observational and statistical significance of the thermal fits in §2. We then discuss some basic properties of the fireball evolution that we can learn from the observed γ -ray behavior in §3 and derive several of the correlations that have been observed for bursts. We discuss our results in §4 and comment on alternative models.

2. Observational Motivation for the Photosphere Model

The photosphere model, which combines a Planck spectrum (see Appendix A) with a power-law, $N_E \propto E^s$, is an alternative way of fitting the observed GRB spectra as compared to the commonly used Band et al. (1993) function. The latter function consists of two power-laws, exponentially connected at the break energy. These two models therefore have the same number of parameters; temperature, power-law slope and two normalizations compared to two power-law slopes, a peak energy and a normalization. The two alternative fitting functions often gives similarly good fits to the data. However, the use of the photosphere model will lead to several important changes in the interpretation of the spectra and their evolution. First we discuss the significance of the fits and later discuss the change in interpretation.

2.1. Significance of the hard spectral slopes

Since synchrotron emission is a very efficient radiation mechanism and is successful in describing the afterglows of GRBs (e.g. Piran (2000)), it has often been assumed that it exclusively can describe the prompt phase as well (Katz 1994; Tavani 1996). The main observational question is therefore whether the hard, sub-peak slopes that have been detected are statistically incompatible with such an interpretation. An optically-thin synchrotron model with the electrons having an isotropic distribution of pitch angles yields a sub-peak power-law with index $\alpha < -2/3$ in the slow cooling regime and $-3/2$ in the fast cooling regime. To answer this question, we revisit the burst of GRB930214 (BATSE trigger # 2193) which is thermal through out its duration (Ryde 2004). Time-resolved spectra from

two different times are shown in Figure 1, where the spectra are plotted in $EF_E \equiv E^2 N_E$ with F_E being the energy flux. The best fit is found with a Planck function. The averaged, reduced χ^2 -value for all the 40 time-resolved spectra fitted with the Planck function, that varies in temperature and amplitude, is $\langle \chi^2_\nu \rangle = 0.998$ for 4687 degrees of freedom (dof) leading to a statistical probability value (p -value) of 0.53. The spectrum in the left-hand panel in Figure 1 is shown as a typical example and has $\chi^2_\nu(\text{dof}) = 0.857(109)$ with $p = 0.86$. Fitting this spectrum with a synchrotron spectrum with a sub-peak slope of $\alpha = -2/3$ (one additional parameter) yields $\chi^2_\nu(\text{dof}) = 1.29(108)$ with $p = 0.02$. These p -values show unequivocally that the Planck function gives a significantly better fit, this even in spite of the fact that it has one parameter less.

Because the optically-thin synchrotron value of $\alpha = -2/3$ is the asymptotic value of the power-law slope, the finite energy range of the observations could have an effect. Another way of quantifying the hardness of the sub-peak emission is therefore to measure the tangential slope at the lowest possible energy to place a lower limit on the asymptotes. Since the α index of the Band et al. (1993) function is determined at $E = 0$ (the asymptote), the actual low-energy power-law indices represented by data with a finite energy range will always be softer (smaller) than the α determined from the fit. Therefore, the actual low-energy spectral behavior of the data can be more accurately described by an “effective” α (α_{eff}) (Preece 1998; Kaneko et al. 2006). The α_{eff} is the logarithmic tangential slope of the fitted Band function at 25 keV, which is the lower energy bound of BATSE Large Area Detectors (LADs). Because $\alpha_{\text{eff}} < \alpha$ for most α values, if α_{eff} significantly exceeds the synchrotron value, the asymptotic low-energy power-law (outside the data energy range) will most likely have an index that also violates the synchrotron limit. Moreover, as an alternative to the Band et al. (1993) function a smoothly-broken power-law (SBPL) model has been successfully used to fit GRB spectra (Preece et al. 1994; Ryde 1999). This model consists of two power laws joined at a certain energy, and a break scale (i.e. a curvature) is determined at the break energy. Thus, unlike the α of the Band function, the low-energy power-law index (λ_1) of this model characterizes the power law represented by the data, unless the break scale is unreasonably large and/or the break energy is very close to the lower energy bound. When LAD data are analyzed with both models, the α_{eff} of the Band function and the λ_1 of the SBPL model are found to be consistent, if both fits are reasonably good (Kaneko et al. 2006). Therefore, by using either the α_{eff} or λ_1 values, lower limits on the asymptotic power-laws can be imposed. Taking the above-mentioned burst, GRB930214 (# 2193), again as an example, all time-resolved spectra within the burst resulted in either α_{eff} or $\lambda_1 > -2/3$ by at least 4.5σ with acceptable fits (resulting χ^2 within 2σ in the χ^2 probability distribution for the given degrees of freedom). The low-energy spectral behavior is thus significantly inconsistent with the synchrotron spectrum, for the entire duration of the burst.

More commonly, bursts only exhibit short intervals of their duration during which the spectra are thermal, most often during an initial interval. An example of such a period is the first 5 seconds of GRB970111 (# 5773). Four of these spectra are shown in figure 2. Here the spectra are plotted as $E^{2/3}N_E$. In such a plot the optically-thin synchrotron slope is a horizontal line. It is clearly seen from the figure that these spectra violate such an interpretation. As mentioned in the introduction these conclusions are reinforced by the observation of similarly hard spectral slopes in this burst by instruments on *Beppo-SAX* (Frontera et al. 2000).

Indeed, a large fraction of all prompt time-resolved spectra have significant deviation of their low-energy indices from values predicted by optically-thin synchrotron emission. Figure 3 illustrates how common this is by showing the distribution of deviations in units of σ of 8459 time-resolved spectra from the BATSE spectral catalog of Kaneko et al. 2006. In this analysis the α_{eff} was used. The fraction of fits that exceed $\alpha = -2/3$ by more than 3σ is 4.8% (407 out of 8459) while the fraction exceeding $\alpha = -3/2$ by more than 3σ is 69.3 % (5870 out of 8459).

From a theoretical point-of-view it is important to know whether the thermal component is described by a Planck function, such as in Ryde (2004, 2005) or whether it is better described by a Wien distribution. The latter arises in a photon-starved atmosphere, dominated by scattering (see further appendix A). The difference between these spectra are only in the asymptotic low-energy slope, $F_E \propto E^2$ and $\propto E^3$, respectively, which in general is difficult to clearly distinguish, unless the observations have high signal-to-noise ratio (SNR) and/or a broad energy band is used. Returning to the spectra in # 2193, a pure Wien function gives a total $\chi^2_{\nu}(\text{dof}) = 1.0607(4687)$ with $q = 0.002$. The expectation value and the variance of the χ^2 distribution is 4687 and thus its standard deviation is 68. The χ^2 -values are $\chi^2_{\text{Planck}} = 4678$ and $\chi^2_{\text{Wien}} = 4972$, that is, a difference of 294. Purely statistically there is therefore a preference for the Planck function. However, it could very well be the case that the Wien peak is accompanied by a power-law component. To investigate this we fit the spectral evolution with a Band et al. (1993) function (with the α -parameter free to vary) combined with a power-law component, and find that the best fit gives a weighted average of $\langle \alpha_w \rangle = +0.98$, but the scatter is large; the un-weighted average is $\langle \alpha \rangle = 1.54$. There are thus time bins with harder than Planck spectra. Indeed, a fit with a Planckian plus a power-law and a fit with a Wienian plus a power-law give similar χ^2 -values. The shape of the thermal component can be compensated for by the non-thermal component, a fact that gives rise to the ambiguity of the fits. It is therefore not possible to clearly determine whether the thermal component of the photosphere model is better described by a Wien or a Planck function. However, an important point is that the evolution of the temperature, $kT = kT(t)$, and the power-law index, $s = s(t)$, are not greatly affected by the shape used for

the thermal component. This is also the case for bursts which have a significant non-thermal contribution, for instance, GRB980306 (# 6630), shown in Figure 4, where it is seen that the kT - and s -evolutions remain quite similar. We note that the Planck function fits have somewhat lower χ^2 -values in this case as well.

Regarding the reliability of the spectral measurements at sub-peak energies it should be noted that it is enhanced by the fact that the photon counts are higher at lower energies, since the spectral photon flux typically goes as the reciprocal of the energy. This is in contrast to the super-peak energies where the number flux falls off rapidly. On the other hand, the instruments always have an energy-dependent photon detection efficiency which decreases both towards the upper and lower ends of the observed energy window. However, it is important to note here that, for BATSE, the high-energy sensitivity drop is more significant compared to the lower energies (within the analysis energy range ≥ 25 – ~ 1800 keV). Indeed, the effective area of the BATSE LAD at 30 keV roughly equals the one at ~ 500 keV (Fishman et al. 1989).

In conclusion, the existence of *time-resolved* spectra that violate the optically-thin synchrotron (isotropic pitch angles) interpretation of prompt phase GRB spectra is therefore made certain beyond any reasonable doubt, in particular since several independent experiments have detected them. The BATSE cases, shown above, clearly and significantly disfavor optically-thin synchrotron emission as a model viable for all time-resolved spectra. However, the data cannot clearly discriminate between Wien and Planck shape of the thermal component, even though, there is a slight favor for the Planckian, in that the fits mostly has a somewhat lower χ^2 -value. Importantly, the temperature and non-thermal power-law evolutions are only marginally affected. To be able to clearly distinguish between a Wien and Planck interpretation, data with broader energy coverage are required since that would permit a stronger constraint to be reached of the power-law slope of the non-thermal component.

2.2. Significance of the decomposition

In the photosphere model the spectra are interpreted as being composed by two separate components. Since this model has the same number of free parameters as the Band function the fits can easily be compared. In most cases the fits are found to be of the same quality (Ryde 2005). Such an example is given by GRB 911031 (# 973), from which a spectrum is shown in the left-hand panel in Figure 5 (the figures are plotted in EF_E units). This burst is equally well fitted by a Band function [$\chi^2_\nu(\text{dof}) = 1.13(108)$] as by a photosphere model [$\chi^2_\nu(\text{dof}) = 1.18(108)$]. For the particular spectrum in the figure we find that $\alpha = -1.0 \pm 0.2$, $\beta = -1.8 \pm 0.1$ and $E_p = 360 \pm 112$, while $kT = 58 \pm 7$ keV and $s = -1.53 \pm 0.04$. However,

in other cases the decomposition is clearly necessary, for instance in the case depicted in the right-hand panel in Figure 5 (GRB 960924; # 5614). Here a Band model fit gives $\chi^2_{\nu}(\text{dof}) = 8(105)$ with $p = 0.00$ and a photosphere model fit gives $\chi^2_{\nu}(\text{dof}) = 1.15(105)$ with $p = 0.14$. The latter fit gives $s = -2.2 \pm 0.1$ and $kT = 112 \pm 1$ keV. The spectrum of GRB 960924 does not have a hard sub-peak power-law slope, as discussed in the cases above, but rather a wavy structure in energy, a feature that is not captured by the Band function or a broken power-law. If this burst had been observed exclusively above 200 keV it would probably be interpreted as being a purely thermal burst, similar to the bursts studied in Ryde (2004). Another example of a burst clearly needing a two-component decomposition is given in Figure 6 (GRB 960530; # 5478). Here the left-hand panel shows the results of a fit with the Band function giving the parameters $\alpha = 1.7 \pm 1.5$ and $\beta = -2.4 \pm 0.3$ while $E_p = 104 \pm 15$ keV [$\chi^2_{\nu}(\text{dof}) = 1.02(109)$; $p = 0.41$]. The right-hand panel shows a fit with the photosphere model, giving $kT = 28 \pm 2$ keV and $s = -0.62 \pm 0.27$ [$\chi^2_{\nu}(\text{dof}) = 0.87(109)$; $p = 0.83$], with more reasonable residuals. In this case, the Band model cannot account for the high-energy rise in the flux beyond 600 keV. This component should be most important at energies beyond the BATSE window studied here. Interestingly, a few super-MeV detections have been made to date which indicate the presence of a possible, additional emission component at these energies (Hurley et al. 1994; Atkins et al. 2000; González et al. 2003). In comparing the two plots in Figure 6, it is important to note the property known as obliging, that is, for models which fit the data badly, the data points tend to be incorrectly depicted. This is a well-known property of the forward-folding technique used for the deconvolution (Fenimore et al. 1983; Bromm & Schaefer 1999). The observed quantity is the photon counts, while the physically interesting photon flux or energy flux are derived quantities which are model dependent. Therefore a plot showing the photon or the energy flux can only be trusted fully if the model fits the data well. However, the statistical fitting is made on the count data and is independent of this effect. GRB960530 is further discussed in the following section.

2.3. Spectral Evolution

The choice of the model used to fit the γ -ray data will lead to distinctly different interpretations of the cause of the apparent, observed, spectral evolution. This is illustrated in Figure 7 which shows the spectral evolution of GRB910927 (# 829). The Band et al. (1993) model is used for the fits in the upper panels whereas the photosphere model was used in the lower-panels. There is an apparent evolution of the low-energy part (sub-peak) of the spectrum. This gives rise to a significant change in the measured α -value, which varies from approximately +1.5 to -0.5 (see Fig. 1 of Crider et al. (1997)). Indeed this burst is often referred to in arguing for that bursts tend to emit in several different radiative regimes

while active. This could, for instance, be due to a variation in the opacity – optically thick to an optically thin regime and/or due to a variation of the pitch angle distribution of the electrons – from a small pitch angle to isotropic regime (Crider et al. 1997; Lloyd-Ronning & Petrosian 2000). However, fitting the spectra with the photosphere model, the picture changes. The apparent spectral evolution is now simply due to changes in temperature and index s , both of which behave similarly to other bursts, that is, a very typical behavior. The left-hand panel in Figure 8 shows the change in temperature of the thermal component, $kT = kT(t)$, which follows the canonical behavior found for thermal pulses, that is, a broken power-law in time. The fit to $kT(t)$ was made with the function derived in Ryde (2004), for which the break-scale may vary. The fit yields that the initial power-law has an index of -0.25 ± 0.02 , which later breaks into a power law with index -0.67 ± 0.13 . The break-scale is described by the parameter $\delta = 0.4 \pm 0.2$, which is defined in equation (6) of Ryde (2004). The time-averaged, reduced χ^2 of the fits is shown in the right-hand panel in Figure 8 and is found to be $\chi^2_{\nu}(\text{dof}) = 0.89$ (3498), which should be compared to the Band function fits which have $\chi^2_{\nu}(\text{dof}) = 0.92$ (3498). It is cases like this one, with an initially high peak-energy and a hard non-thermal component, that gives rise to pulses which have an initial thermal phase. We therefore conclude that the strong α -evolution, that is often attributed to bursts, is actually an artifact of the evolving relation between the thermal and the non-thermal components, combined with the limited spectral energy-range of the observations.

The majority of bursts have spectra for which the α -index is either a constant or becomes softer with time, like in the cases discussed above. However, in GRB960530 (# 5478) α becomes apparently harder (α becomes larger) which is demonstrated in the left-hand panel in Figure 9. We will now show that this power-law evolution again can be naturally ascribed to an artifact of the empirical fit with the Band function, and that it simply reflects the underlying variation in the components of the photosphere model and their relative strengths. Figure 10 shows four time-resolved spectra to which the photosphere model was fitted. In the last two spectra, the power-law component is important in determining the spectral shape at the highest energies. The temperature decays again as a broken power-law with slopes ~ -0.4 and ~ -0.7 (middle panel in Fig. 9). The thermal flux is indeed dominant initially (Ryde & Battelino 2005), however, the power-law index, s , behaves differently from other bursts in that it becomes harder with time; s makes a jump from ~ -1.5 to -0.67 at approximately 5 seconds after the trigger (right-hand panel in Fig. 9). The thermal component is thereby revealed at low energies, with its hard Rayleigh-Jeans tail. This leads to the large α -values that are found when the Band function is fitted to the spectra. The change in s from ~ -1.5 to $\sim -2/3$ can be interpreted as that the synchrotron cooling frequency of the electrons passes through the band-pass, towards higher energies, at around 5 s. Such a behavior can be imagined if the amount of dissipated energy going into the

magnetic fields decreases with time. Since the error bars are somewhat large, this conclusion is by necessity not beyond challenge. As can be seen in Figure 9, the index s is also consistent of being constant at, say, ~ -1.5 . The whole time evolution can in fact be fitted to a model with s fixed at -1.5 . This model then has only *three* free parameters and gives an excellent fit to the whole spectral evolution with a total $\chi^2_{\nu}(\text{dof}) = 0.997(1870)$. The thermal component, on the other hand, behaves similarly to other bursts with a broken power-law decay in time. It should also be noted here that with a pure synchrotron model, instead of the photosphere model, the observed behavior of GRB960530 is difficult to explain.

2.4. Distribution of the Power-Law Indices

Ryde (2005) used the photosphere model to study a sample of the 25 strongest pulses in the Kocevski, Ryde, & Liang (2003) catalogue. In the left-hand panel in Figure 11 is shown the distribution of the power-law indices, s , of the non-thermal component that was found for all the 347 time-resolved spectra that were modelled. Note that s most often varies throughout a burst as well. Interestingly, the distribution is peaked at $s = 1.5 - 1.6$. This is the value expected if most spectra are due to a population of fast cooling electrons ($s = -1.5$) or acceleration in relativistic shocks due to first order Fermi process; $s = -(\hat{p} + 1)/2 = -1.6$. Here \hat{p} is the power-law index of the electron energy distribution. We also note that no cases are harder than the slow-cooling synchrotron slope of $-2/3$. A larger sample is presented in Battelino et al. (in prep.) with a similar distribution. This distribution should be compared to the right-hand panel in the figure which shows the distribution of the Band α -values from the catalogue of Kaneko et al. (2006). Here many cases have spectra harder than $\alpha = -2/3$ and thus the distribution crosses the 'line-of-death' of the optically-thin synchrotron model. The distribution peaks at ~ -0.8 , which does not have an immediate physical meaning. Early suggestions included thermal bremsstrahlung (with a Gaunt factor of 1) of an optically-thin hot plasma which yields $\alpha = -1$ (Rybicki & Lightman 1979). However such a mechanism is too inefficient to be able to give rise to GRB spectra (Liang 1982).

2.5. Merits of the Photosphere Model

Optically-thin synchrotron emission is excluded as a viable model for the prompt phases in a fair fraction of the time-resolved spectra in GRBs. Indeed a large variety of spectral shapes and evolutions have been described in the literature. We argue that the photosphere model gives a reasonable description, however, it should be noted that other models have

been proposed. For instance, small pitch-angle synchrotron emission and inverse Compton emission from mono-energetic soft photons are alternative scenarios that give hard low-energy spectral slopes. See further details on this in §4.

We find the following main features when the photosphere model is used to interpret the γ -ray data of GRBs.

(i) For most cases the fits are as good as the fits made using the Band model. In some cases the χ^2 -values are indeed lower for the photosphere model.

(ii) The photosphere model can naturally incorporate all types of spectral behaviors, even bursts which are consistent with optically-thin synchrotron emission. In particular, it naturally explains the existence of pulses that are thermal throughout their duration (Ryde 2004), simply as cases for which the non-thermal component is weak or does not affect the spectrum in the observed energy range. Some bursts are thermal only initially, while others are thermal only at the end. The different realizations is naturally explained by the change in relative strength between the two spectral components. The theoretical interpretation of the variation in component strengths is discussed in §3.4. This means that we have one and the same model for all bursts.

(iii) The strong α -evolution, that is found in many bursts when the Band model is used, has been discussed extensively in works trying to explain the emission process at play. We argue that this evolution in fact does not need to reflect the emission process itself but rather the variation of the two components and their relative strength.

(iv) The distribution of the spectral index of the non-thermal component, here modelled by a power-law across the observed window, is peaked at approximately -1.5. This is the value that is expected from a population of fast cooling electrons emitting, e.g synchrotron radiation. Furthermore, the index ~ -1.6 is expected from relativistic shock accelerated electrons in the slow cooling regime. Such a preferred value is not found from the Band α -distribution. The interpretation of the change in s can be that the synchrotron frequency passes through the observed window (Ryde 2004; Battelino 2006) or, alternatively, it can be interpreted as the spectrum actually changes due to increased cooling, see further discussion in Ryde et al. (2006, in prep.)

(v) The photon index of the non-thermal component are mainly smaller than $-2/3$, that is, the 'line-of-death' for optically-thin synchrotron emission is not crossed.

(vi) Interestingly the temperature, kT , evolves similarly for most bursts, except for a few cases. This is also the case for bursts which, a priori, do not require a thermal component, since their spectra can equally well be fitted by a optically-thin synchrotron model. For

these burst, the temperature of the thermal component still behave in the canonical way; having a break in the cooling behavior.

Finally, models invoking thermal emission naturally give rise to correlations between flux and spectral peak energy, i.e. temperature. Such correlation are observed for an ensemble of bursts (Lloyd-Ronning & Petrosian 2000; Amati et al. 2002) as well as during the course of one single burst (Ryde & Svensson 2000; Borgonovo & Ryde 2001). Also the clustering of the peak energy that is observed can be a natural consequence. These issues are discussed in more detail in §§3.3 and 3.5.

3. Theoretical Implications of Strong Thermal Emission

We interpret the thermal component as emission from the fireball photosphere, the point at which the outflow becomes optically thin. Quite general conclusions can then be drawn from the fact that we detect strong thermal emission, which is shown in the next section. In appendix B, the basic evolution of the fireball is presented and we will describe how it can be used to interpret the existence of and the behavior of the thermal component.

3.1. The Photosphere

The three, main unknown parameters of the outflow at the point where the thermal emission is emitted is the Lorentz factor, Γ , the distance from the central engine, R , and the comoving lepton density, n' . However, these properties can be deduced using the observables, mainly the temperature, T , pulse length, t_{pulse} , total energy emitted, E_{tot} and the associated solid angle, Ω , into which the outflow is collimated. The latter two quantities are related by the isotropic equivalent energy as $E_{\text{iso}} = E_{\text{tot}} \times 4\pi/(2\Omega)$. In the following, we will denote the frame of reference at rest with the progenitor as the lab frame and the comoving frame is at rest with the outflow. Quantities in the latter frame are primed. Finally, observed quantities are made in the observer frame.

We have three equations to solve for the three unknowns.

- (i) At a certain radius R the optical depth to electron scattering, given by

$$\tau_{\text{hor}} = \sigma_{\text{T}} n' l'_{\text{hor}}, \quad (1)$$

reaches unity and the entrained photons expand freely towards the observer maintaining their thermal distribution. Here, σ_{T} is the Thompson optical depth and l'_{hor} is the horizon length, that is, the distance travelled by a photon within the shell during the lab frame time

R/c , the dynamical time-scale. This corresponds to a comoving time $t' = R/c\Gamma$ and thus a comoving distance

$$l'_{\text{hor}} = \frac{R}{c\Gamma} c = \frac{R}{\Gamma} \quad (2)$$

(ii) We assume that the energy density in the black-body emission, $U'_{\text{BB}} \equiv aT'^4$ ($a = 7.56 \times 10^{-15}$ erg cm $^{-3}$ K $^{-4}$) is equal to the radiation energy density $U'_{\text{BB}} = U'_{\text{rad}}$, which in its turn is proportional to the internal rest mass energy density $U'_{\text{rm}} = n'm_p c^2$, where m_p is the mass of the proton: $U'_{\text{BB}} = \xi n'm_p c^2 = \xi m_p c^2 \frac{\tau_{\text{hor}} \Gamma}{\sigma_T R}$, where ξ is the proportionality factor and includes possible dilution factors in a scattering atmosphere. Equation (2, 1) was used in the last step. With $T' = T/\Gamma$ this gives an expression for the Lorentz factor

$$\Gamma^5 = \frac{T^4 a \sigma_T}{\xi m_p c^2 \tau_{\text{hor}}} R \quad (3)$$

The minimal Γ is given by $\tau_{\text{hor}} = 1$.

(iii) The total energy emitted in the shell is

$$E_{\text{tot}} = 2\Gamma \Delta' \Omega R^2 U'_{\text{rm}} (1 + \kappa) = 2\Gamma^3 \Delta \Omega R m_p c^2 \frac{\tau_{\text{hor}}}{\sigma_T} (1 + \kappa) = 2\Gamma^3 c^3 m_p \Omega R \frac{\tau_{\text{hor}}}{\sigma_T} t_{\text{pulse}} (1 + \kappa) \quad (4)$$

where we used that the comoving shell width $\Delta' = \Gamma \Delta$ and that the energy is divided into two jets on either side of the burst. κ holds the ratio between relativistic particles/photons and cold particles. In the last step we used that fact that $\Delta = ct_{\text{pulse}}^{\text{obs}}$, since the pulse duration in this model is the light crossing time of the lab frame width of the shell. Rewriting this we get an expression for the distance from the central engine to the emission site as

$$R = \frac{E_{\text{tot}} \sigma_T}{2\Gamma^3 c^3 m_p \Omega \tau_{\text{hor}} t_{\text{pulse}} (1 + \kappa)} \quad (5)$$

which, used with equation (3), gives

$$\Gamma^8 = \frac{a \sigma_T^2}{4\pi c^5 m_p^2 (1 + \kappa) \xi} \times \frac{T^4 E_{\text{iso}}}{\tau_{\text{hor}}^2 t_{\text{pulse}}} \quad (6)$$

This gives that ($\tau_{\text{hor}} = 1$ for the photosphere)

$$\Gamma = 307 \left(\frac{1}{(1 + \kappa) \xi} \right)^{1/8} \left(\frac{T}{100 \text{keV}} \right)^{1/2} \left(\frac{E_{\text{iso}}}{10^{53} \text{erg}} \right)^{1/8} \left(\frac{t_{\text{pulse}}}{10 \text{s}} \right)^{-1/8} \quad (7)$$

which is a typical value one finds using the compactness argument (see e.g. Piran (2000)). Combining equations (3) and (5) again we also get that

$$R^{8/3} = \frac{\xi m_p c^2 \tau_{\text{hor}}}{T^4 a \sigma_T} \left[\frac{E_{\text{tot}} \sigma_T}{2c^3 m_p \Omega \tau_{\text{hor}} t_{\text{pulse}} (1 + \kappa)} \right]^{5/3}, \quad (8)$$

which gives a radius of

$$R = 4.0 \times 10^{11} \text{cm} \left(\frac{1}{(1 + \kappa)} \right)^{5/8} \left(\frac{E}{10^{53}} \right)^{5/8} \left(\frac{T}{100 \text{keV}} \right)^{-3/2} \left(\frac{t}{10 \text{s}} \right)^{-5/8} \quad (9)$$

This value corresponds approximately the radius of a Wolf-Rayet star, generally assumed to be the progenitor.

It is interesting to note that equations (7) and (9) follow directly from the existence of strong thermal emission in the spectra. These general results now correspond to $n' = 1.15 \times 10^{15} \text{cm}^{-3}$, $l' = 4 \times 10^9 \text{cm}$, and $\Delta = 3 \times 10^{11} \text{cm}$. Note that $\Delta \sim R$ and $l = R\Gamma^{-2} \sim \Delta\Gamma^{-2}$, that is, the horizon length is much smaller than the wind width, indeed by a factor of 10^{-5} . Furthermore, we have that $U'_{\text{BB}} = aT'^4 = 1.56 \times 10^{14} \text{erg/cm}^3$ and $M_{\text{tot}} = n'm_p dV' = 3.4 \times 10^{-7} M_{\odot}$. The dimensionless entropy of the outflow is therefore $\eta \equiv E_{\text{tot}}/M_{\text{tot}}c^2 = 313$.

3.2. A Toy Model

A steady flow (constant energy) will give rise to constant observer quantities, such as the temperature, since the photosphere would lie at the same radius (see eq. 33), and thus no spectral evolution would be present. Variation in the outflow is therefore necessary since spectral evolution does indeed take place. In this paper, we will focus on the correlations between flux and peak energy (e.g. Ryde & Svensson (2000); Borgonovo & Ryde (2001); Amati et al. (2002); Ghirlanda (2003)) and a detailed analysis on the temporal behavior of the temperature is deferred to a future publication. One possibility for this variation is that the dimensionless entropy of the material that is injected into the jet at R_i (from where the outflow starts to accelerate) varies with time

$$\eta(t) = \frac{E_i(t)}{M_i(t) c^2} = \frac{U_{\text{rad},i}(t)}{n'_i(t) m_p c^2} \quad (10)$$

Such a variation will lead to varying $R_{\text{eq}}(t)$ (see eq. [32]) and thereby a varying $R_{\text{ph}}(t)$ as discussed below, reproducing the observed temperature behavior. During the acceleration phase the comoving temperature decreases linearly with radius, $T' \propto R^{-1}$ as discussed in Appendix B. Therefore the radiation energy-density is given by

$$U_{\text{rad}}(R) = aT'^4(R) = aT'_i{}^4 \left(\frac{R}{R_i} \right)^{-4} \quad (11)$$

Since $n' \propto R^{-3}$ (from mass conservation in eq. [27]), the rest-mass energy-density is then given by

$$U_{\text{rm}}(R) = n'(R)m_p c^2 = m_p c^2 n'_i \left(\frac{R}{R_i} \right)^{-3} \quad (12)$$

Defining R_{eq} as the radius at which $U_{\text{rm}} = U_{\text{rad}}$, we have

$$R_{\text{eq}} \propto \frac{T_i'^4}{n_i'} \quad (13)$$

The entropy injected into the outflow can depend differently on the rest-mass energy and the radiation for different bursts. Energy dissipation will increase the radiation energy-density through various emission processes in the neighborhood of R_i . If the dissipation occurs through collisions of denser regions (e.g. shells), the amount of energy dissipation should depend non-linearly on the volume-averaged particle density, since several regions are involved. Furthermore, the energy extraction processes around the newly formed black hole are, in general, complex and the radiation processes involved are often expected to have a strongly non-linear behavior (neutrino annihilation, electron-positron pair cascades, etc.) which therefore could account for such non-linear relations as well. In either scenario such behavior can be parameterized according to the following toy model

$$U_{\text{rad},i} \propto U_{\text{rm},i}^\zeta \Leftrightarrow T_i'^4 \propto n_i'^\zeta \quad (14)$$

In other words we let $\eta(t)$ vary with time and require that $\eta(t) = U_{\text{rad},i}(t)^{1-1/\zeta}$. Accordingly, bursts which have large values of the power-law index ζ thus have a flow in which the variation in entropy mainly results in a variation in comoving temperature.

An alternative description is that R_{eq} varies due to changes in the energy to mass ratio relation during the dissipation in the outflow itself. The temperature and density inhomogeneities can then be parameterized by $T' = T'_{\text{eq},0} \hat{T}'$ and $n' = n'_{\text{eq},0} \hat{n}'$, now assuming constant initial flow conditions in equations (11, 12). In this case the R_{eq} -condition, $(T')^4 \propto n'$, gives a similar ratio as in equation (13) with \hat{T}' and \hat{n}' instead of T_i' and n_i' . The following analysis and discussion will therefore be correspondingly similar between these scenarios.

Using the toy model relation [eq. (14)] in equation (13) thus yields

$$R_{\text{eq}} \propto n_i'^{\zeta-1} \quad (15)$$

Furthermore, since the comoving lepton density varies according to $n'(R) = n_i (R/R_i)^{-2}$ beyond R_{eq} , equations (1) and (2) gives that $\tau_{\text{hor}} = \sigma_{\text{T}} n_i' R_i^2 / R \Gamma$. The thermal photons are released from the outflow when the opacity over a horizon length corresponds to $\tau_{\text{hor}} = 1$. Therefore,

$$R_{\text{ph}} = \sigma_{\text{T}} R_i^2 \frac{n_i'}{\Gamma} \propto \frac{n_i'}{R_{\text{eq}}} \propto n_i'^{2-\zeta} \quad (16)$$

since $\Gamma \propto R_{\text{eq}}$ (eq. [32]). Equations (15) and (16) thus parameterizes R_{eq} and R_{ph} with the initial comoving lepton density n_i' (alternatively \hat{n}').

3.3. The Expected Hardness-Intensity Correlation (HIC)

During the coasting phase ($R > R_{\text{eq}}$ and $\Gamma = \text{constant}$) the observed peak in the spectrum, which is directly proportional to the temperature, is given by $T_{\text{ph}}^{\text{obs}} = \Gamma T'_{\text{ph}} = \Gamma T'_{\text{eq}} \left(\frac{R_{\text{ph}}}{R_{\text{eq}}} \right)^{-2/3}$ as discussed in Appendix B. The ratio of the photospheric radius and the saturation radius is thus given by

$$\frac{R_{\text{ph}}}{R_{\text{eq}}} = \left(\frac{T_{\text{eq}}^{\text{obs}}}{T_{\text{ph}}^{\text{obs}}} \right)^{3/2} \quad (17)$$

which leads to that the luminosity is given by

$$L \propto \Sigma (T_{\text{ph}}^{\text{obs}})^4 \propto (R_{\text{ph}}/\Gamma)^2 T_{\text{ph}}^4 \propto (T_{\text{eq}}^{\text{obs}})^3 T_{\text{ph}} \propto (T_i^{\text{obs}})^3 T_{\text{ph}} \quad (18)$$

where Σ is the emitting surface subtended by the opening angle of Γ^{-1} , with $\Gamma \propto R_{\text{eq}}$. We also used the fact that during the acceleration phase $T_{\text{eq}}^{\text{obs}} = \Gamma(R_{\text{eq}})T'_{\text{eq}} = \Gamma(R_i)T'_i = T_i^{\text{obs}}$. Furthermore, by combing equations (15) and (16) with equation (17) we find that

$$T_{\text{ph}}^{\text{obs}} = T_i^{\text{obs}} n_i^{(4\zeta-6)/3} \propto T_i^{(19\zeta-24)/3\zeta}. \quad (19)$$

where we have used the toy model relation between initial temperature and density, equation (14). This relation can then be inserted in equation (18) to find

$$L \propto T_{\text{ph}}^{\frac{28\zeta-24}{19\zeta-24}}. \quad (20)$$

Such a relation for the hardness-intensity correlation (HIC) is indeed found for individual pulse structures. The power-law indices are found to have a large dispersion with values centered around approximately 2 (see Fig. 3 in Borgonovo & Ryde (2001)). These values are, however, for the total flux, i.e. both the thermal and the non-thermal flux. The observed values of the exponent in equation (20), will therefore be somewhat larger, since the non-thermal flux increases in relative strength as the temperature drops (see below in §3.5). The exponent as a function of ζ is shown by the solid curve in Figure 12. The interpretation is therefore that the majority of bursts have $\zeta \sim 2$, while a few bursts have larger values; as the parameter ζ tends to infinity the exponent tends to $28/19 = 1.47$. For the former bursts this, for instance, would correspond to approximately equal density regions colliding while for the latter bursts the dissipation leads to that the variation in radiation energy-density (T_i or \hat{T}) is much dominant over that in the rest-mass energy-density (or n'_i or \hat{n}). We also note that if ζ approaches $24/19 = 1.26$ the luminosity would change without any temperature change, that is, without any significant spectral evolution. This is not observed.

3.4. Ratio between the thermal and the non-thermal emission

The non-thermal component of the spectra is assumed to arise at a later time, farther out. In this optically-thin region the kinetic energy, which is still residing in the outflow can be dissipated by, for instance, shocks or magnetic reconnections in which electrons are accelerated to non-thermal distributions. These are cooled by emitting synchrotron and/or inverse Compton emission. The non-thermal emission will therefore be delayed compared to the thermal light curve with a time scale that corresponds to the time it takes the shell to move from the photospheric radius to the dissipation region.

$$\Delta t^{obs} = \frac{R_{diss.} - R_{ph}}{2c\Gamma^2} \sim 0.17 \text{ s} \left(\frac{\Delta R}{10^{14}\text{cm}} \right) \left(\frac{\Gamma}{100} \right)^{-2} \quad (21)$$

GRB pulses that are initially thermal are, in part, a manifestation of such a delay. An example of such a time delay is shown in Figure 13 in Ryde (2004). However, with a smaller ΔR , say 10^{13}cm , such a time delay would be difficult to detect in general.

As mentioned above, Ryde (2005) showed that the variety in spectral shapes that are seen in GRBs is, in part, attributed to a variation in strength between the thermal and the non-thermal component in the spectra. In the model presented here this translates into a variation between the thermal energy and the kinetic energy at R_{ph} . This will depend on the relation between the saturation radius and the radius at which the photosphere occurs, which is given by equations (15) and (16) as

$$\frac{R_{ph}}{R_{eq}} \propto T_i^{(12-8\zeta)/\zeta} \quad (22)$$

In more detail, since $kT \propto \rho^{1/3}$ we have that the ratio between the energy density in thermal radiation and non-thermal radiation, the latter assumed to be proportional to the kinetic energy and thereby ρ , is given by

$$\frac{U_{BB}}{U_{non-th}} \propto \frac{aT^4}{\rho} \propto T \quad (23)$$

as the fireball expands. If the photospheric radius is close to the saturation radius then the thermal and non-thermal energies are equally large (per definition) but if $R_{ph} \gg R_{eq}$ then the ratio will have decreased due to the scaling in equation (23). This means that the relative strength of the thermal component compared to the non-thermal component in GRBs vary from burst to burst and within a burst due to variations in the ratio R_{ph}/R_{eq} , i.e. the location of the photosphere relative to the saturation radius. We therefore have that

$$\frac{L_{th}}{L_{non-th}} = \frac{T_{ph}}{T_{eq}} = \left(\frac{R_{ph}}{R_{eq}} \right)^{-2/3} \propto T^{\frac{16\zeta-24}{19\zeta-24}} \quad (24)$$

where we have used equation (17) and in the last step equations (19) and (22). The dependence of the exponent is shown by the dashed curve in Figure 12. For large values of ζ the ratio in the exponent goes as $\propto T^{16/19} = T^{0.84}$. The dispersion of this exponent is somewhat smaller as is evident from the figure. As the observed temperature drops in a burst (e.g. due to varying T_i or \hat{T}) the non-thermal luminosity should become increasingly more important. An example of this type of behavior, with a power-law relation between the flux ratio and the temperature, is shown in the right-hand panel in Figure 13 for GRB921207 (# 2083).

3.5. Luminosity-peak energy (Amati/Ghirlanda) relation

In the discussion above the properties intrinsic to individual bursts have been in focus, for instance, discussion on the correlation between hardness and intensity (HIC; Ryde & Svensson (2000); Borgonovo & Ryde (2001)). When studying the relationship between average properties of a sample of bursts, normalization of the intrinsic properties must be done. During the acceleration phase, the normalization is given by the radius where the acceleration starts, R_i , so that $\Gamma = \Gamma_i(R_{\text{eq}}/R_i)$. From equation (4) we have that

$$E_{\text{iso}} = 4\pi\Delta\Gamma^2 R^2 n' m_p c^2 \propto \Delta\Gamma^2 R_i^2 n'_i \propto R_{\text{eq}}^2 n'_i \Delta \propto \frac{T_i^8}{n'_i} \Delta \propto T_i^{\frac{8\zeta-4}{\zeta}} \Delta \quad (25)$$

where we have made use of equation (13). If we assume that Δ does not vary significantly between bursts then we have with equation (19) that $E_{\text{iso}} \propto T_{\text{ph}}^{\frac{24\zeta-12}{19\zeta-24}}$. While this is the total energy, the observed, radiated energy is a fraction $\epsilon \propto T_{\text{ph}}/T_{\text{eq}} \propto T^{(16\zeta-24)/(19\zeta-24)}$ (from eq. 24) or $E_{\text{rad}} = \epsilon E_{\text{iso}} \propto T^{\frac{40\zeta-36}{19\zeta-24}}$ which is proportional to the luminosity. For $\zeta \gtrsim 3$ this relation reproduces the observed luminosity–peak-energy relation noted by Amati et al. (2002), however see also Nakar & Piran (2005). Indeed, for ζ tending to infinity the exponent is $40/19 = 2.1$. Since the scatter around the Amati-relation is somewhat large, the modified relation introduced by Ghirlanda et al. (2004) can be used instead: $E_{\text{iso}} t_{\text{jet}} \propto E_p^2 \propto T^2$, with t_{jet} being the jet break time, which implies instead that the global parameter $t_{\text{jet}} \Delta$ does not vary significantly between bursts.

In conclusion, the simplified toy model that was introduced above reproduces the main characteristics of the observed burst behaviors. For most cases the variation in radiation energy-density of the outflow needs to be stronger than that in the particle energy-density. Obviously, more work is needed to make this description into a realistic model. However, the basic features of the behavior are well described by the above framework.

4. Discussion

Even though a major part of the total energy in a GRBs is emitted during the prompt phase, consensus has not yet been reached regarding the emission sites and mechanisms. For a model to successfully describe this phase the following observational facts has to be appropriately addressed:

- (i) Existence of hard spectral slopes below the peak energy, i.e., large values of the parameter α , giving rise to the line-of-death problem.
- (ii) Beside producing both hard and soft sub-peak spectra, the model should be able to reproduce more complicated spectral shapes such as the ones in Figs. 5 and 6. In addition, the shape of the spectrum around the peak that should not be too broad. The values of the model parameter that are inferred by the observations should have a distribution that has a reasonable explanation.
- (iii) The *evolution* of the spectral shape. This could be represented by parameters of non-thermal models, such as the Band-function α , or parameters of the photosphere model, such as kT and/or s . In the former case the α parameter translates into physical parameters depending on the chosen model.
- (iv) The distribution of peak energies; why the peaks mainly fall into the range they do.
- (v) The correlation between peak energy and flux during a burst, i.e. the hardness-intensity correlation, HIC, which is characteristic for every burst (Ryde & Svensson 2000; Borgonovo & Ryde 2001).
- (vi) The Amati/Ghirlanda (Amati et al. 2002; Ghirlanda 2003) relations for an ensemble of bursts should be predictable on reasonable grounds by the model.
- (vii) Burst and pulse durations. The derived radii at which the emission process takes place as well as the derived Lorentz factors should not lead to the compactness problem.
- (viii) The microphysics implied: does the cooling occur in situ with the acceleration or do they occur in separated regions? What underlying particle distributions is needed to describe the observations, given the acceleration and dissipation processes?

Here we have presented a physical framework that addresses most of these points. In particular, it can explain pulses that are thermal through out their duration. The analysis made above in §2 and in Ryde (2004, 2005) indicate that the temperature has a canonical behavior with the temperature decaying as a broken power-law, independent of the apparent behavior of the burst. In the model presented here this simply reflects the temperature distribution within the shell. These results are for the class of long bursts (see e.g. Balázs

et al. (2003)) and the corresponding behavior for short and intermediate duration bursts (Horváth et al. 2006) will be discussed elsewhere.

For the bursts discussed in this paper, the peak energy was observed to be within the BATSE energy range. However, the case could very well be that kT is actually outside of that range, say at energies lower than 10 keV. In such a case the spectrum within the BATSE window would mainly reflect the non-thermal emission. The thermal component would reveal itself by an upturn in the spectrum at low energies, similarly to the case in the lower right-hand panel in Figure 10. We have also assumed that the thermal emission is not greatly affected by a scattering photosphere, to the extent that it pertains its Planckian shape as indicated by the observations. However, strong scattering can be important and has been discussed elsewhere (Rees & Mészáros 2005; Pe’er et al. 2005).

In this connection, it is worth mentioning the work by Vetere et al. (2005) who studied rapidly varying burst which are accompanied by a slowly varying component. They suggest that the latter component is thermal and associated with the photosphere while the former, variable component is due to external shocks, giving non-thermal spectra. Such a picture fits in nicely with the model presented above and deserves further investigation.

What alternative models does there exist? As shown above a purely optically-thin synchrotron (OTS) emission (isotropic pitch angles) is rejected purely by the spectral shapes. In the canonical diffusive shock model the typical acceleration times are much shorter than the typical synchrotron cooling times. However, the acceleration and the cooling do not necessarily need to occur in the same place. This will lead to electrons acquiring a fast cooling distribution, since the cooling time is shorter than the dynamical time scale (Ghisellini et al. 2000). This results in a spectral softening, with an expected $\alpha = -1.5$ instead of $-2/3$. OTS then becomes even less plausible. Another concern with the OTS is that the peak energy will depend on several of the model parameters; Γ , γ_{\min} , and B_{\perp} making it hard to get the preferred energy breaks as observed. Lloyd-Ronning & Petrosian (2000) discussed the possibility that the hard spectral slopes are due to synchrotron self-absorption, i.e. the electrons absorb the photons themselves, which would lead to harder spectral slopes in the photon fluxes; E^1 or $E^{3/2}$ (Rybicki & Lightman 1979). They noted that to get a high optical-depth to self-absorption in the BATSE energy range somewhat extreme parameters have to be used, in particular, one needs to invoke a very high magnetic field. At a dissipation distance of 10^{13} cm, particle density of 10^8 cm^{-3} , and with $\Gamma = 1000$ one would need approximately 10^8 G. Note that the generation of magnetic fields in the outflow, in particular such strong fields, is not well understood (see e.g. Frederiksen et al. (2004)). Furthermore, the Compton y -parameter will in such a case be of order unity which thus reduces the efficiency in the observed range since emission will be up-scattered to higher energies (Kumar

1999).

Another efficient radiative mechanism is inverse Compton scattering: the gamma-ray spectrum could instead be an inverse Compton image of the synchrotron spectrum, now located in the optical since the energy increase goes as γ^2 . Such a synchrotron self-Compton model was explored by Panaitescu & Mészáros (2000). The low-energy slope will be the same as for the synchrotron seed spectrum, $\alpha < -2/3$. But if the latter is self-absorbed, a situation which now requires much lower magnetic field strengths, the low-energy spectrum could be as hard as $\alpha = 0$ (Jones 1968). However, as Baring & Braby (2004) pointed out, the spectrum around its peak is notably broader than what is observed. Alternatively, the inverse Compton emission could be seeded by soft photons with a narrow energy distribution, i.e. a quasi-mono-energetic distribution, producing a less broad spectrum and with a limiting value again at $\alpha = 0$. Compared to synchrotron emission such an emission mechanism also alleviates the requirements on the magnetic field strength.

Yet another alternative is the small pitch-angle synchrotron-emission (SPA) (Epstein 1973; Epstein & Petrosian 1973) and similarly jitter radiation (Medvedev 2000, 2006), which produce hard spectral slopes as well, $\alpha < 0$. Here the γ -dependant distribution of pitch angles is needed as well as a scenario to set up a distribution for which the pitch angles are not much greater than γ^{-1} . This could be done by rapid cooling and inefficient diffusion transverse to the magnetic field (Lloyd-Ronning & Petrosian 2000).

The latter two models are thus the main contenders for describing the prompt phase with a purely non-thermal model. Diffusive shock acceleration (Fermi processes) is assumed to accelerate electrons from a shocked thermal population into a non-thermal distribution, which cool by these mechanisms and emit the observed radiation. Baring & Braby (2004) noted, however, that both these emission processes need an almost purely non-thermal electron distribution to be able to fit the observed spectra. This is difficult to reconcile with shock models, which often have a strong contribution of a thermal population. We note here that the non-thermal component in the photosphere model, presented in this paper, does not have its break energy within the BATSE window. Therefore such fitting constraints are not found and a thermal component of the electron population can very well be present in that case.

It will be necessary to have a broader energy coverage to be able to reach firm conclusions on the actual spectral shape in the X- and γ -rays, and thereby conclusively identifying the emission process. The *GLAST* satellite is expected to provide better clues with its much broader energy range compared to presently available observations.

We wish to thank Drs. Asaf Pe’er, Stefan Larsson, and Attila Mészáros for useful

discussions and comments on the manuscript. Financial support for this research was given by the Swedish Research Council, the Swedish National Space Board, Swedish Foundation for International Cooperation in Research and Higher Education (STINT), NASA through contract NAG 5-13286 and NSF under grant AST 03-07376.

APPENDIX A

SPECTRUM OF THE THERMAL COMPONENT

In the photosphere model, discussed above, the thermal component is the dominating feature of the spectrum, dictating the peak evolution. Its energy flux spectrum has a general form described by

$$F_E(T) = \frac{2}{h^2 c^2} \frac{E^3}{e^{E/kT-\mu} - 1}, \quad (26)$$

where T is an effective temperature, k is Boltzmann's constant = 1.38×10^{-16} erg K⁻¹, and μ is the dimensionless chemical potential. For photon statistics with unrestricted amount of photons $\mu = 0$ and the photon distribution will reach a thermodynamic equilibrium so that equation (26) reduces to the Planck distribution, $F_E \propto E^3 [\exp(E/kT) - 1]^{-1}$ (Planck 1901), which for $E \ll kT$ has an asymptotic behavior of $\propto E^2$. However, in a pure scattering atmosphere, for instance, the photons can gain energy from hot electrons via inverse-Compton scattering. The spectrum will then be distorted since the number of photons has to be conserved, that is, photons are neither created nor destroyed in the scattering process. This restriction (Bose-Einstein statistics) leads to a non-zero (negative) chemical potential μ and the photons will arrive at a statistical equilibrium instead. For $E > kT(1+\mu)$, we can neglect the unity in the denominator and it simplifies to the Wien distribution $F_E \propto E^3 [\exp(-E/kT)]$ (Wien 1896), which asymptotically approaches $\propto E^3$ towards lower energies. This is thus the resulting spectrum that is established if there is a mismatch between the number of photons and the energy that is distributed among them.

APPENDIX B

FIREBALL EVOLUTION

We envision the following scenario in which GRBs are formed. As the black hole is created during the core collapse of the progenitor star (most probably a Wolf-Rayet star¹),

¹expected to be the progenitor star of the special type of Supernova Ic that is referred to as a collapsar

gravitational and rotational energy is extracted and creates a hot, optically thick gas. The large amounts of energy per baryon involved will make it quickly expand under its own pressure, accelerating the baryons to relativistic velocities (Paczynski 1998). This requires that the surrounding material is not too thick for the fireball to be halted. The collapsar model provides a depleted funnel through the progenitor, which is created along the rotation axis since angular momentum in the equatorial region prevents the matter to collapse on a short time scale. In addition a precursor outburst can clear the way for subsequent outflows. The funnel will focus the fireball into a collimated outflow with an opening angle of Ω .

The energy injection at the central source, or engine, lasts over a period of Δ/c where Δ is the lab frame width of the shell that is thus emitted. The rate of injection can vary on a shorter time scale than this and is parameterized by variations in the dimensionless entropy η (defined in eq. [10]) or equivalently in the temperature, T' and the density of baryons, n' . Conservation of mass is described by

$$\Sigma \rho' \Gamma v = \dot{M} \quad (27)$$

where Σ is the emitting surface, \dot{M} is the rate of baryonic matter that is injected to the outflow, ρ' is the rest mass density, and v is the velocity. Conservation of energy gives

$$\Sigma(U' + P')\Gamma^2 c = H \quad (28)$$

where P' is the pressure, and H is the rate of thermal energy ejected by the central engine (erg/s) which, during the course of the flow, is transformed into kinetic energy. If we assume the outflow to be a relativistic ideal fluid, for which the internal energy density is $U' = 3P' > \rho' c^2$, we can simplify equation (28) to

$$U' = \frac{3}{4} \frac{H}{\Sigma \Gamma^2 c} \quad (29)$$

which together with the conservation of mass (eq. 27) gives

$$\frac{U'}{\rho'} = \frac{3}{4} \frac{H}{\dot{M} \Gamma}. \quad (30)$$

For a photon gas (with $\tau \gg 1$) we have that $U' \propto \rho'^{4/3}$ so equation (30) gives that $U'^{1/4} \propto \Gamma^{-1}$. Since $U' = aT'^4$, the temperature, in the observer frame would be $T^{\text{obs}} = T'\Gamma = \text{constant}$. If this relation is used together with equation (29), which is equivalent to $T' \propto (\Gamma^2 \Sigma)^{-1/4}$ we find that $T' \propto \Sigma^{-1/2} \propto R^{-1}$ and $\Gamma \propto R^1$. During the acceleration period the Lorentz factor increases linearly with radius. The typical temperature during the acceleration phase would be (independent of R)

$$kT^{\text{obs}} \sim \frac{k}{1+z} \left(\frac{H}{4\pi R_i^2 c a} \right)^{1/4} = 100 \text{ keV} \left(\frac{1+z}{2} \right)^{-1} \left(\frac{H}{10^{51} \text{ erg/s}} \right)^{1/4} \left(\frac{R_i}{10^8 \text{ cm}} \right)^{-1/2}, \quad (31)$$

assuming an initial radius where the acceleration starts where $\Gamma = 1$, R_i . As above we define the distance R_{eq} as the radius at which the rest mass energy density and radiation energy density are equal (assuming $\tau \gg 1$). The flow saturates not far beyond this radius at $R_{\text{sat}} \sim R_{\text{eq}}$ and coasts along with a constant Lorentz factor. We then have that

$$\Gamma = \eta = \Gamma_i \frac{R_{\text{sat}}}{R_i} \sim \frac{R_{\text{eq}}}{R_i} \quad (32)$$

with $\Gamma_i \sim 1$. During the coasting phase we also have that $U' = \rho' c^2 + 3P' \sim \rho' c^2$ which gives that $\Gamma \sim \text{constant}$ since equation (30) gives that $U' \propto \rho'/\Gamma$. Mass conservations also gives that $\rho' \propto R^{-2}\Gamma^{-1}$ which combined with $kT' \propto \rho'^{1/3}$ (the adiabatic relation for a photon gas) gives

$$kT^{\text{obs}} = kT'\Gamma \propto R^{-2/3} \quad (33)$$

since Γ is constant.

REFERENCES

- Amati et al. 2002, A&A, 390, 81
- Atkins, R., et al. 2000, ApJ, 533, L119
- Balázs, L. G., Bagoly, Z., Horváth, I., Mészáros, A., & Mészáros, P. 2003, A&A, 401, 129
- Band, D., et al. 1993, ApJ, 413, 281
- Baring, M.G., & Braby, M.L. 2004, ApJ, 613, 460
- Barraud, C., et al. 2003, A&A, 400, 1021
- Battelino 2006, Diploma thesis, Stockholm University.
- Borgonovo, L., & Ryde, F. 2001, ApJ, 548, 770
- Bošnjak, Ž. M. 2005 PhD thesis, SISSA, Italy
- Bromm, V. & Schaefer, B. 1999, ApJ, 520, 661
- Bussard, R.W. 1984, ApJ, 284, 357
- Crider, A., et al. 1997, ApJ, 479, L39
- Daigne, F. & Mochkovitch, R. 2002, MNRAS, 336, 1271

- Drenkhahn, G., & Spruit, H. C. 2002, *A&A*, 391, 1141
- Epstein, R. I., & Petrosian, V. 1973, *ApJ*, 183, 611
- Epstein, R. I. 1973, *ApJ*, 183, 593
- Fenimore, E. E., Klebesadel, R. W., & Laros, J. G. 1983, in *Gamma-Ray Astronomy in Perspective of Future Space Experiments* (New York: Pergamon), 201
- Fishman, G.J., & Meegan, C.A. 1995, *ARAA*, 33, 415
- Frederiksen, J. T., Hededal, C. B., Haugbølle, T., & Nordlund, Å. 2004, *ApJ*, 608, L13
- Frontera, F., Amati, L., Costa, E. et al. 2000, *ApJSS*, 127, 59
- González, M. M., Dingus, B. L., Kaneko, Y., Preece, R. D., Dermer, C. D., & Briggs, M. S. 2003, *Nature*, 424, 749
- Ghirlanda, G., Celotti, A., & Ghisellini, G. 2003, *A&A*, 406, 879
- Ghirlanda, G., Ghisellini, G., & Lazzati, D. 2004, *ApJ*, 616, 331
- Ghisellini, G., Lazzati, D., Celotti, A., & Rees, M. J. 2000, *MNRAS*, 316, L45
- Ghisellini, G., Celotti, A., Lazzati, D. 2000, *MNRAS* 313, L1
- Horváth, I., Balázs, L. G., Bagoly, Z., Ryde, F., & Mészáros, A. 2006, *A&A*, 447, 23
- Hurley K. et al. 1994, *Nature*, 372, 652
- Jones, F. C. 1968, *Phys. Rev: Lett.*, 167, 1159
- Kaneko, Y. 2005, PhD thesis, University of Alabama
- Kaneko, Y., Preece, R.D., Briggs, M.S., Paciesas, W.S., Meegan, C.A. & Band, D.L. 2006, *ApJS*, in press (astro-ph/0605427)
- Katz, J. I. 1994, *ApJ*, 432, L107
- Kocevski, D., Ryde F., & Liang E., 2003, *ApJ*, 596, 389
- Kobayashi, S., Ryde, F., & MacFadyen, A. 2002, *ApJ*, 577, 302
- Liang, E. P. 1982, *Nature*, 299, 321
- Lloyd-Ronning, N. & Petrosian, V. 2000, *ApJ*, 543, 722

- Lloyd-Ronning, N. M., Petrosian, V., & Mallozzi, R. S. 2000, ApJ, 534, 227
- Medvedev, M. V. 2006, ApJ, 637, 869
- Medvedev, M. V. 2000, ApJ, 540, 704
- Mészáros, P. 2002, ARA&A, 40, 137
- Mészáros, P., Ramirez-Ruiz, E., Rees, M. J., & Zhang, B. 2002, ApJ, 578, 812
- Mészáros, P., & Rees, M. J. 2000, ApJ, 530, 292
- Nakar, E. & Piran, T. 2005, MNRAS, 360, L73
- Pacholczyk, A. G. 1970, *Radio Astrophysics* (San Francisco: W. H. Freeman and Co.)
- Panaitescu, A., & Mészáros, P. 2000, ApJ, 544, L17
- Pe’er, A., & Waxman, E. 2004, ApJ, 613, 448
- Pe’er, A., et al. 2005, in prep.
- Petrosian, V., & Liu, S. 2004, ApJ, 610, 550
- Piran, T. 2000, Phys. Rep., 333, 529
- Planck, M. 1901, Ann. Physik, 4, 553
- Preece, R.D., Briggs, M.S., Mallozzi, R.S., & Brock, M.N., 1994, “WINDows Gamma SPECTral ANALYSIS (WINGSPAN)”
- Preece, R.D., Briggs, M.S., Mallozzi, R.S., Pendleton, G.N., Paciesas, W.S., & Band, D.L. 1998, ApJ, 506, L23
- Preece, R. D., Briggs, M. S., Mallozzi, R. S., Pendleton, G. N., Paciesas, W. S., & Band, D. L. 2000, ApJSS, 126, 19
- Ramirez-Ruiz, E., & Lloyd-Ronning, N.M. 2002, NewA, 7, 197
- Rees, M. J. & Mészáros, P. 2005, ApJ, 628, 847
- Rybicki, G. B., & Lightman, A. P. 1979, *Radiative Processes in Astrophysics* (New York: Wiley)
- Ryde F. 1999, ASP Conf. Proc., 190, 103

- Ryde, F. 2004, *ApJ*, 614, 827
- Ryde, F. 2005, *ApJ*, 625, L95
- Ryde, F. et al. 2006, *MNRAS*, in prep.
- Ryde, F., & Battelino, M. 2005, *Il Nuovo Cimento*, 28C:3, 335
- Ryde, F., & Svensson, R. 2000, *ApJ*, 529, L13
- Strohmayer, T. E., Fenimore, E. E., Murakami, T., & Yoshida, A. 1998, *ApJ*, 500, 873
- Tavani, M. 1996, *ApJ*, 466, 768
- Thompson, C. 2005, *ApJ*, submitted
- Thompson, C., Mészáros, P., Rees, M. 2006, *ApJ*, submitted
- Wien, W. 1896, *Wiedemanns Annalen der Physik und Chemie*, 58, 662
- Zhang, B. & Mészáros, P. 2002, *ApJ*, 581, 1236

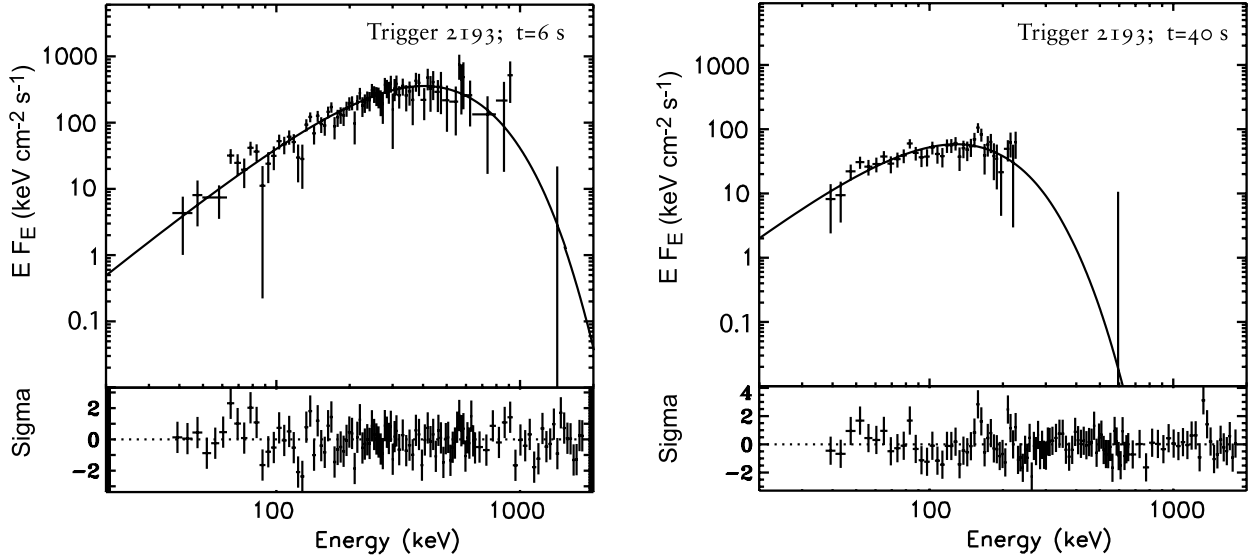


Fig. 1.— Spectra with hard sub-peak slopes. Two time-resolved spectra from GRB930214 (BATSE trigger 2193) from 6 and 40 seconds after the trigger (sub-second integration time). Note that the spectra are fitted well with a Planck function, both in the Rayleigh-Jeans portion of the spectrum with $\alpha = +1$ and in the Wien portion with a fast avoidance of flux. The temperature has changed between the measurements (see also Ryde (2004)). The spectral data points have been rebinned to a higher signal-to-noise ratio to increase clarity. The original energy resolution is kept in the fitting and in the residual plots.

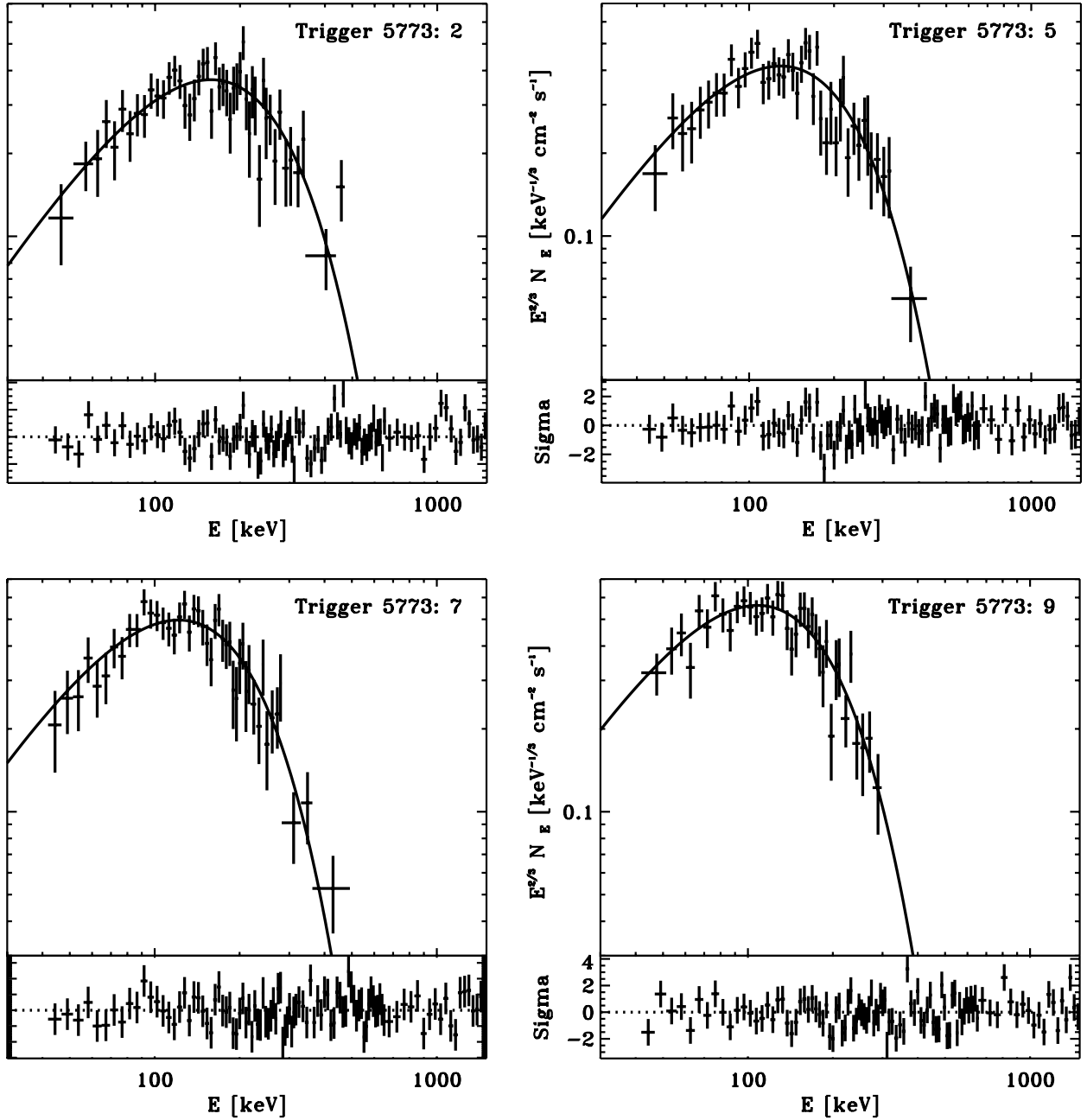


Fig. 2.— Four time-resolved spectra of GRB 970111 (#5773) during the first 5 seconds of the burst. The numbers in the upper right-hand corner refer to the sequel number of time-bin used (see figure 13 in Ryde 2004). Note that the ordinate is given by $E^{2/3}N_E$, which for instance has the consequence that optically-thin synchrotron emission ($\alpha = -2/3$) will appear as a horizontal line in the plot. The low-energy slope of these spectra are clearly significantly harder than this, which is also seen from the analysis in the text.

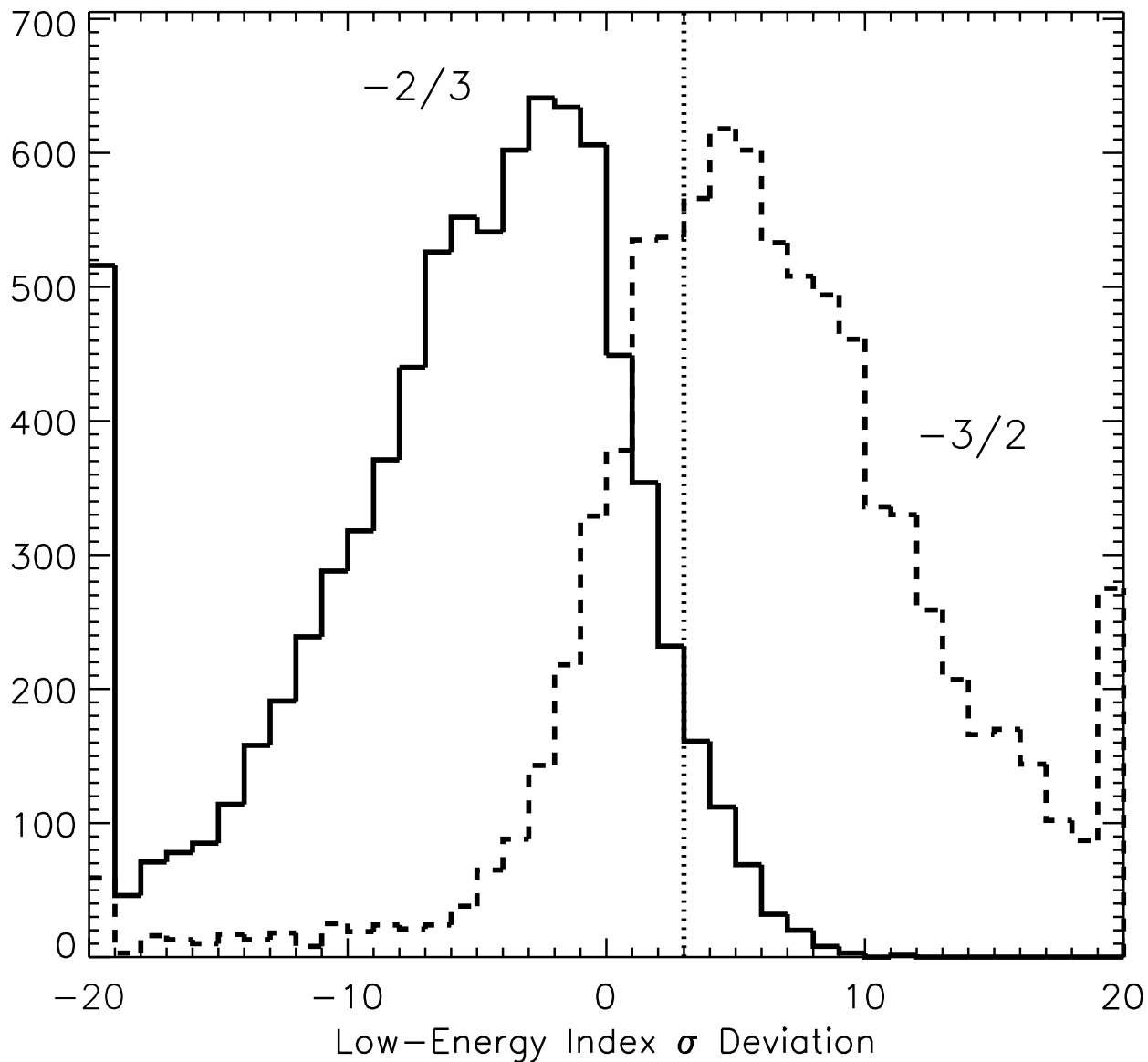


Fig. 3.— Distribution of deviations (in units of σ) of the low-energy indices of 8459 time-resolved spectra from values predicted by optically-thin synchrotron emission: $\alpha = -2/3$ (solid line) and $\alpha = -3/2$ (dashed line). Positive 3σ deviation is marked by the dotted line, i.e. spectra to the right of the line are incompatible with synchrotron radiation. Overflow counts at each end of the distribution are summed up in the ultimate bins.

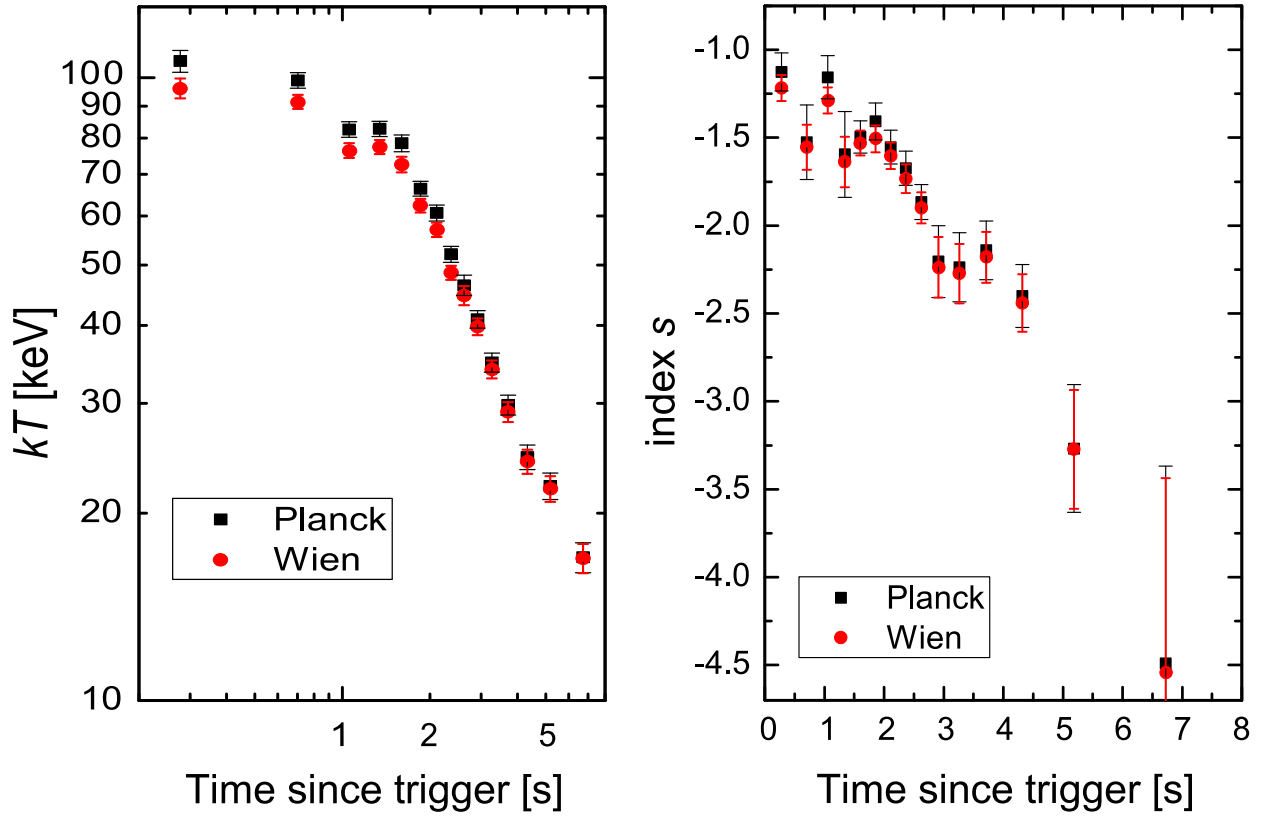


Fig. 4.— The temperature and s -evolution for GRB 980306 (#6630). The black dots (square) are for a photosphere model in which the thermal component is described by a Planck function, while the red dots (round) uses a Wien function. 1- σ errors.

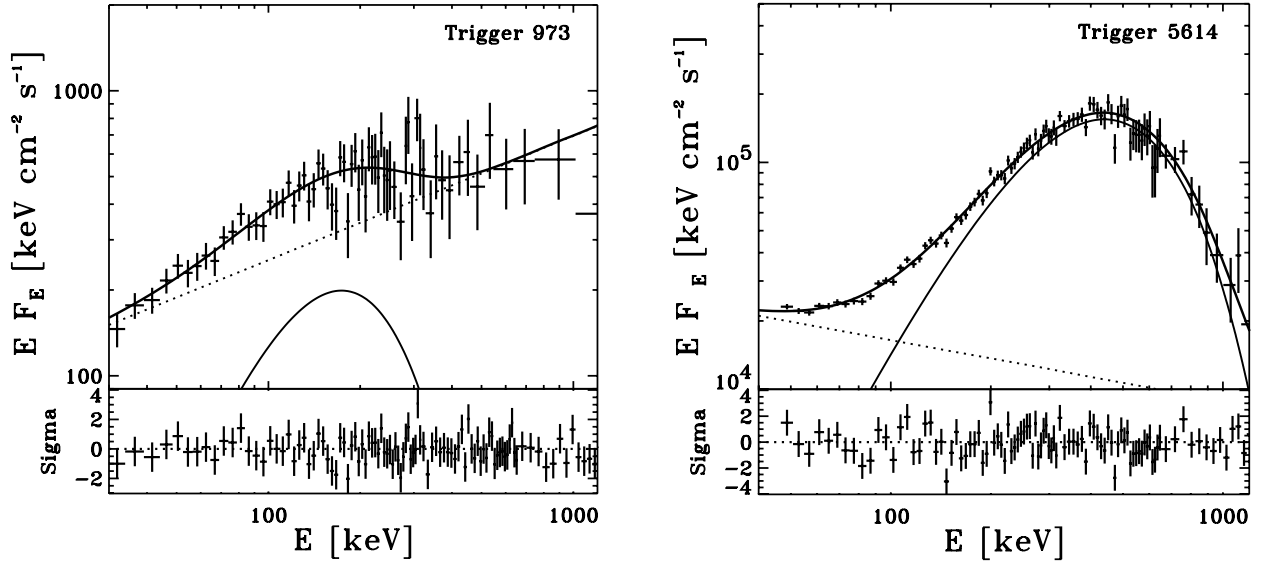


Fig. 5.— *Left panel:* A spectrum from GRB911031 (#973; 3 s after the trigger) fitted with the photosphere model (Ryde 2004), with a power-law slope of $s = -1.53 \pm 0.04$ and $kT = 56 \pm 7$ keV. A fit using the Band et al. (1993) model results in a similarly good fit, with $\alpha = -1.0 \pm 0.2$ and $\beta = -1.8 \pm 0.1$. *Right panel:* Time-resolved spectrum from GRB 960924 (#5614, ~ 9 s after the trigger). The burst is totally dominated by the thermal component above 200 keV. The two components of the photosphere model is clearly needed; $\chi_\nu = 1.15(105)$ compared to $\chi_\nu^2 = 8(105)$ for a Band function fit. The spectral data points have been rebinned to a higher signal-to-noise ratio to increase clarity. The original energy resolution is kept in the fitting and in the residual plots.

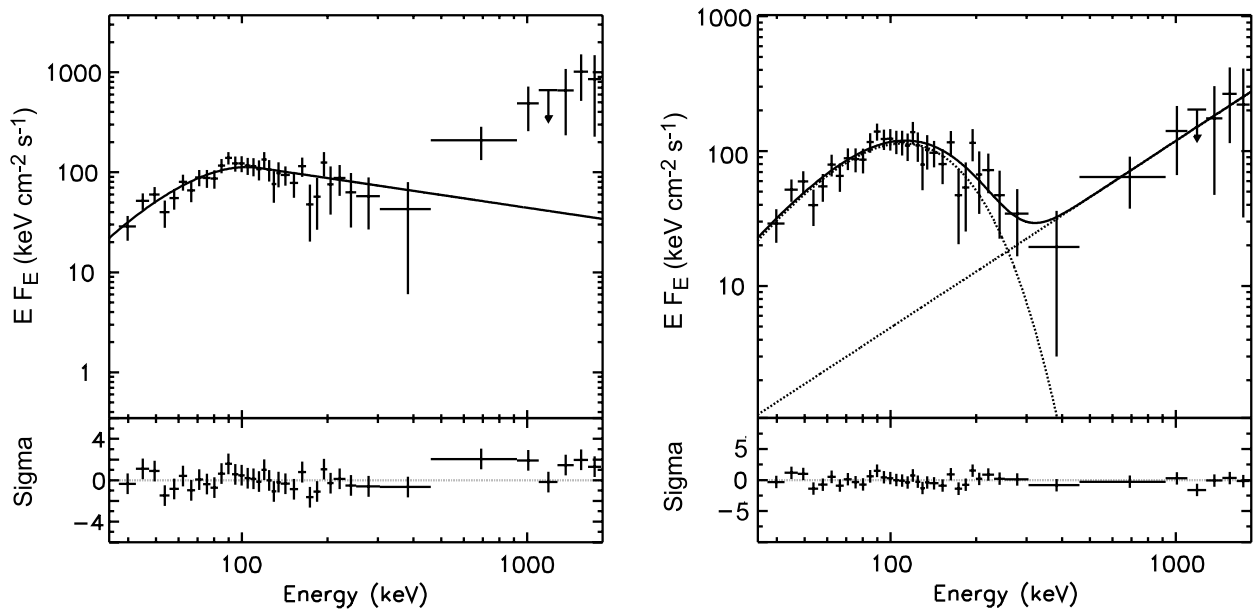


Fig. 6.— The spectrum from GRB960530 (#5478; 6 s after the trigger) fitted with (left panel) the Band et al. (1993) model with $\alpha = 1.7 \pm 1.5$ and $\beta = -2.4 \pm 0.3$ and (right panel) the two-component model (Ryde 2004), with a power-law slope of $s = -0.62 \pm 0.27$. Note the obliquing of the data points (Fenimore et al. 1983; Bromm & Schaefer 1999).

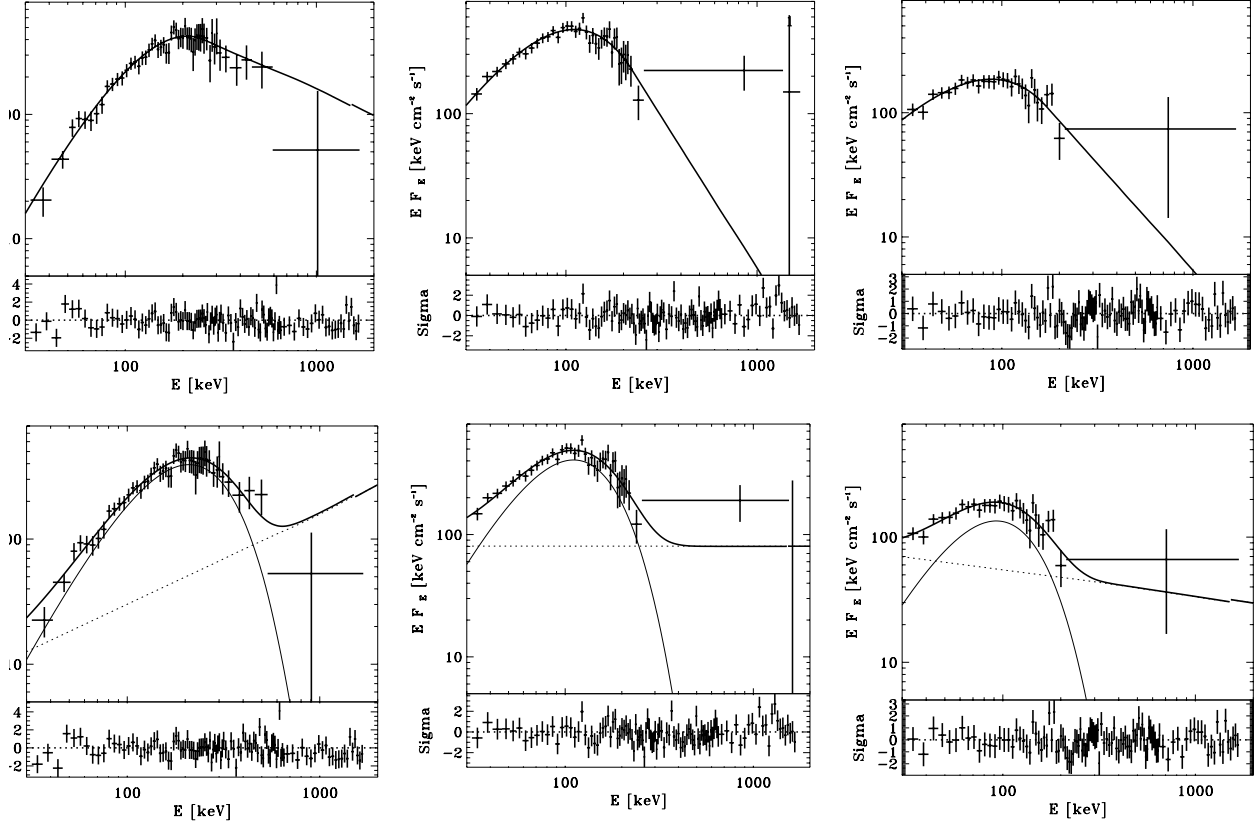


Fig. 7.— Spectral evolution of GRB 910927 (# 829), represented by time bins at 1, 6, and 10 seconds after the trigger. *Upper panels:* the spectral evolution that is found by using the Band model results in evolution of α and E_p . In particular, the α -evolution is noteworthy. *Lower Panels:* The evolution found by using the photosphere model becomes very typical, in particular in the evolutions of kT and s . The data points have been rebinned to $\text{SNR} = 3$. See the text for further details.

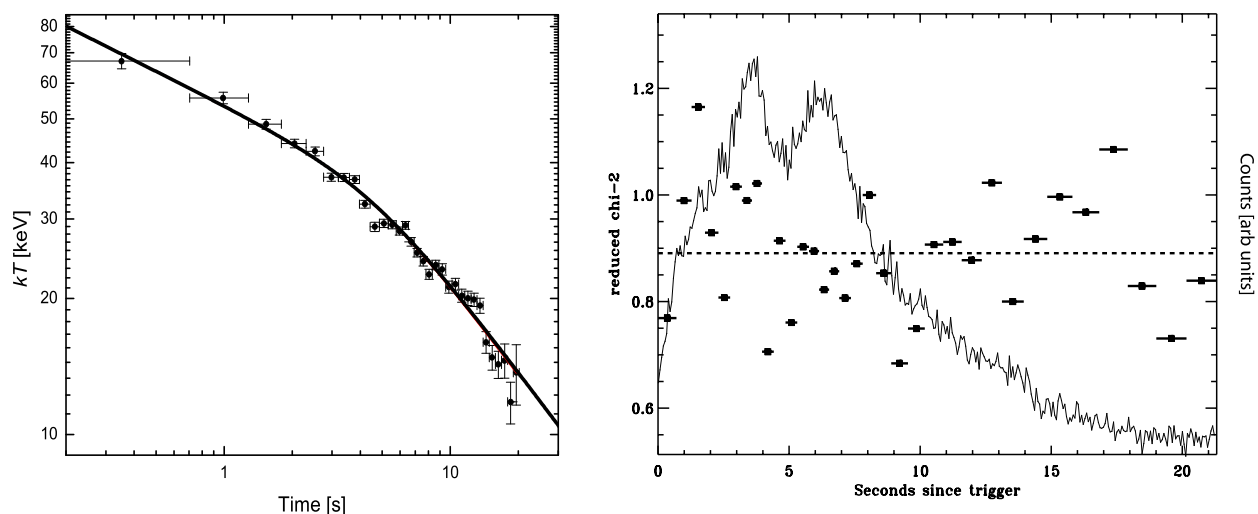


Fig. 8.— Spectral evolution of GRB910927 (# 829) found from using the photosphere model. *Left panel:* Temperature evolution of the thermal component. The solid line represents the best fit to a smoothly broken power-law function. The early time power-law index is $a = -0.25 \pm 0.02$ and the late time index $b = -0.67 \pm 0.13$. *Right panel:* reduced- χ^2 values for the time-resolved fits. The total value is $\chi^2_\nu = 0.89$ for 3498 degrees of freedom (dashed line). The solid line shows the count light curve.

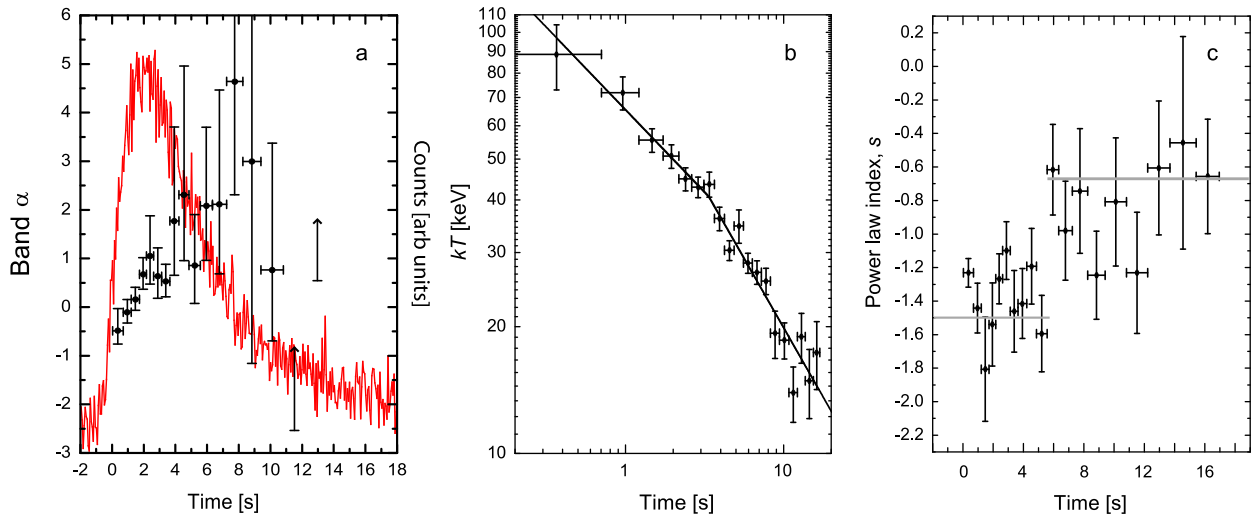


Fig. 9.— (a) Count light curve and the low-energy power-law index, α . Fitting the time-resolved data of GRB960530 (# 5478) with the Band function, the α becomes harder at the end of the burst. This is the opposite behavior to most bursts with strong spectral evolutions. $1\text{-}\sigma$ errors. (b) The temperature of the thermal component evolves as a broken power-law in time. (c) The non-thermal power-law index, s makes a jump from ~ -1.5 to ~ -0.67 at approximately 5 s. The grey lines indicate these theoretical values.

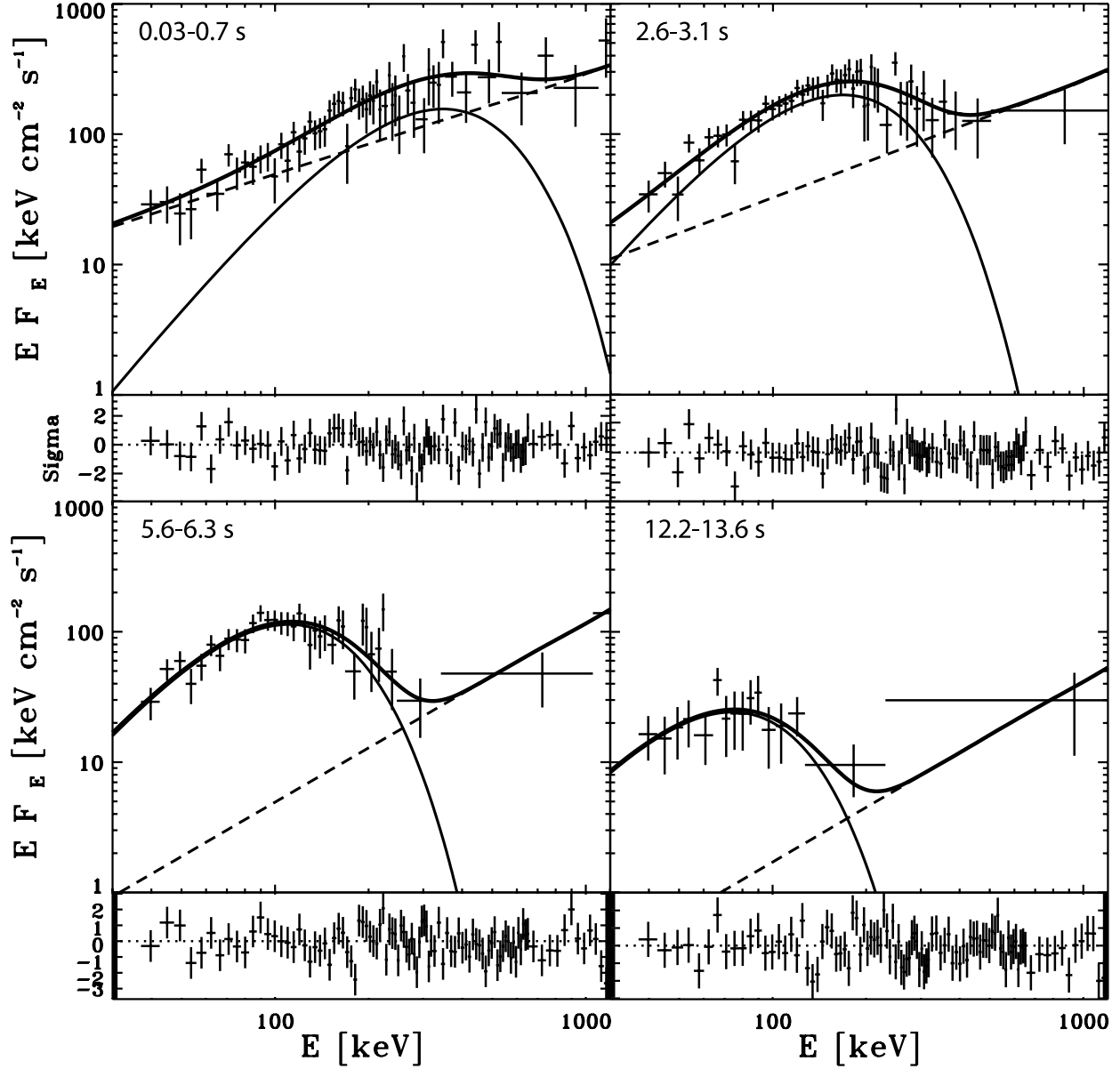


Fig. 10.— Four time-resolved spectra of GRB960530 (# 5478) fitted with the photosphere model of Ryde (2004). The non-thermal component is depicted by the dashed line and the time bins (relative to the trigger) that are used for the fits are given in the upper left-hand corner of each panel. The non-thermal spectral component is important in determining the shape of the spectrum at the end of the pulse.

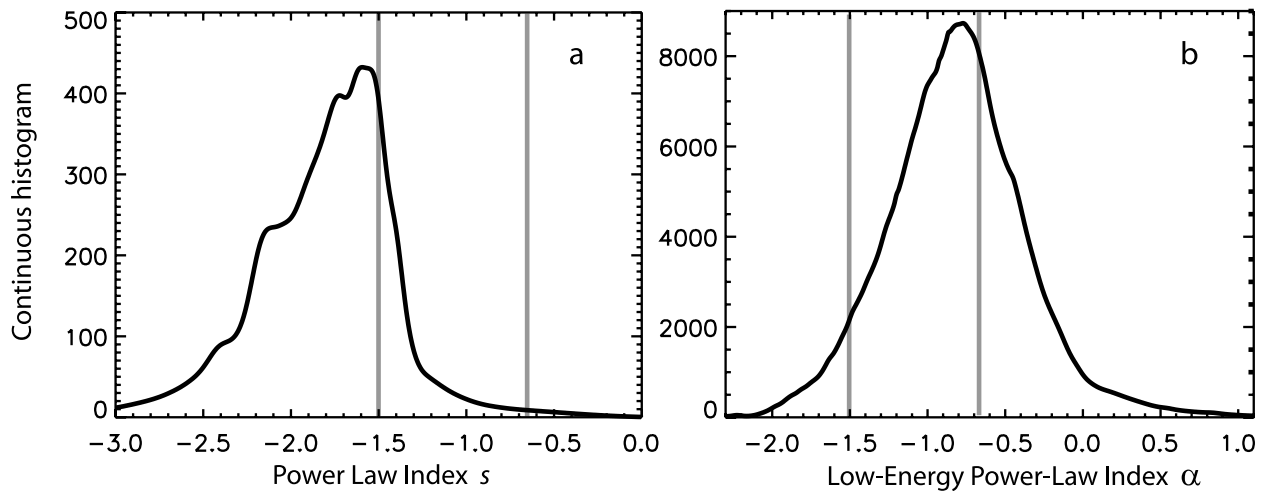


Fig. 11.— (a) Continuous histogram of the power-law index, s , of the non-thermal component of the 25 bursts studied in Ryde (2005). The distribution peaks between -1.5 and -1.6 . (b) Corresponding histogram of the low-energy power-law index α for the 8459 time-resolved spectra in the catalogue of Kaneko et al. (2006). This distribution can be compared to the ones in Figure 3. The grey lines indicate the indices $-2/3$ and -1.5 expected for synchrotron emission with slow and fast cooling electrons.

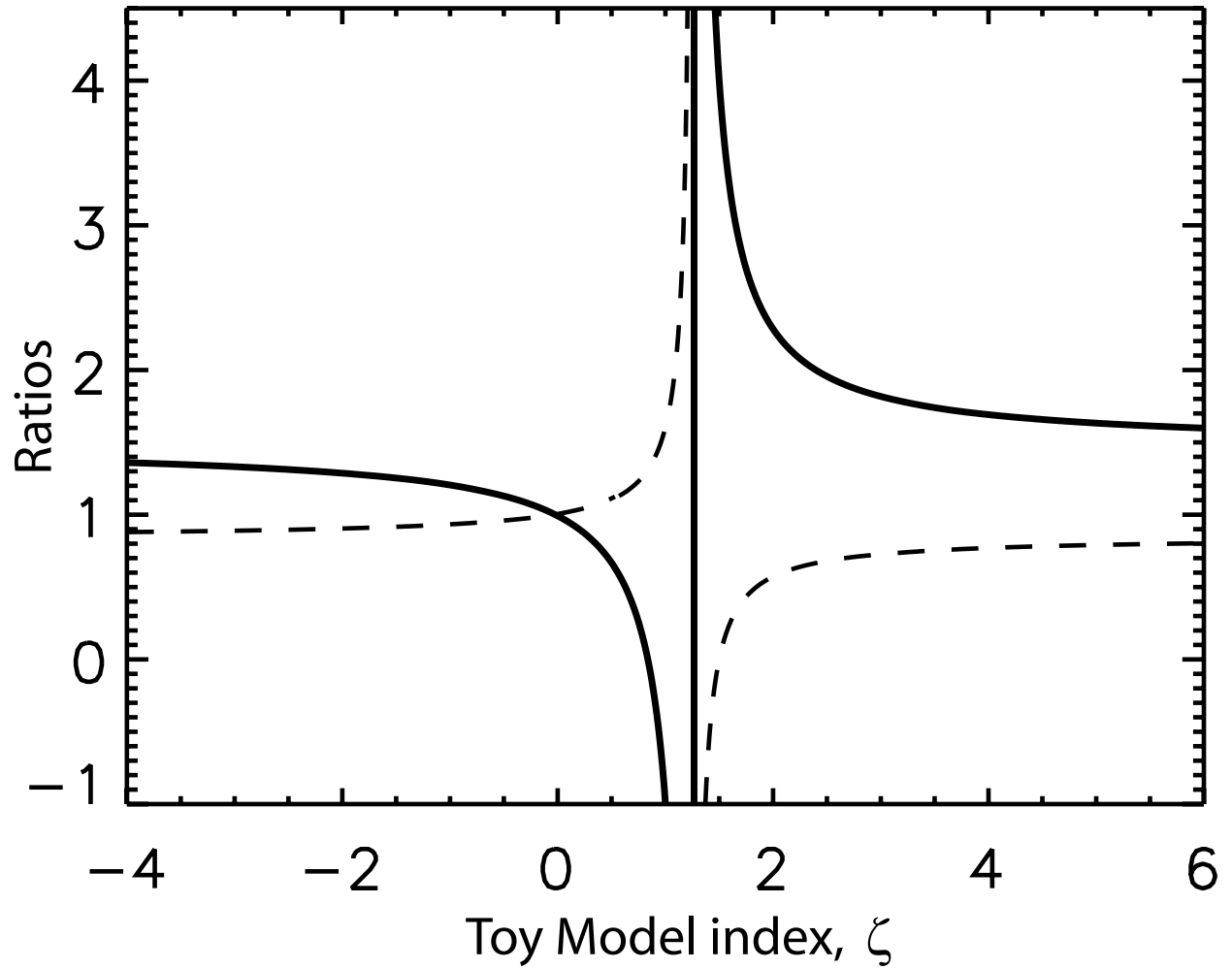


Fig. 12.— The behavior of the exponent in equation 20 (bold, solid line) and equation 24 (thin, dashed line) as a function of parameter ζ of the toy model in equation (14).

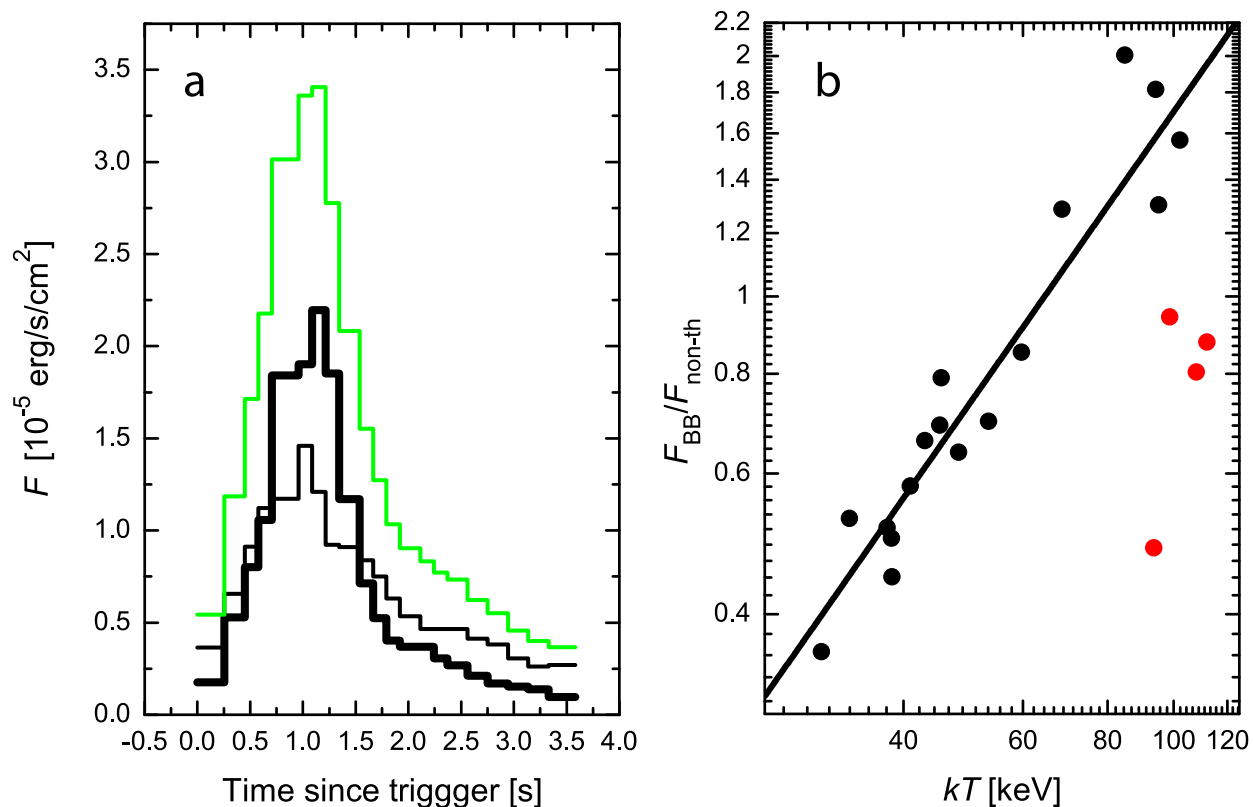


Fig. 13.— Example of the energy flux behavior illustrated by GRB921207 (# 2083) (a) Energy fluxes in units of $10^{-5} \text{ erg/s/cm}^2$: Thermal (solid), non-thermal (thin), and total (grey). (b) Ratio of the thermal and the non-thermal fluxes as a function of temperature, kT . The grey points are for the rising phase of the pulse. The power-law relation is close to linear with the power-law index having a value of 1.2 ± 0.6 .